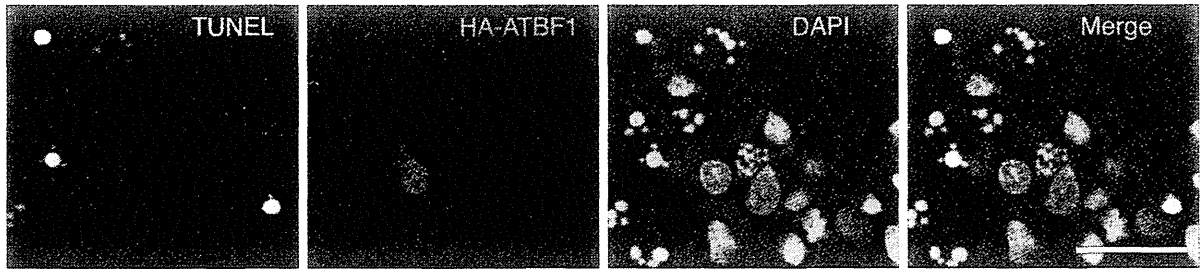

Figure 5 Overexpression of HA-tagged ATBF1 itself in primary cortical neurons did not induce apoptosis. TUNEL of primary cortical neurons transfected with HA-tagged ATBF1. The cells were transiently transfected with HA-tagged ATBF1. Twenty-four hours after transfection, TUNEL was performed, and then the cells were stained with the anti-HA antibody to detect transfected HA-ATBF1. Scale bars: 25 μm.

dead cells treated with Aβ1-42, etoposide, or homocysteine at concentration as low as 1 μM. These findings indicated that treatment with ATM inhibitors protect against Aβ1-42-, etoposide-, or homocysteine-induced neuronal death. Next, we assessed the effect of siRNA-mediated ATBF1 knockdown on Aβ1-42-induced neuronal death after treatment with caffeine or KU55933. As shown in Figure 6C and Additional file 3, there are no significant differences in the percentage of survival between ATBF1 siRNA-transfected neurons with treatment of caffeine or KU55933 and those without treatment with caffeine or KU55933. These findings indicate that ATBF1 is required for neuronal death in response to Aβ1-42 treatment, which could be dependent on ATM signaling.

ATBF1 interacted with phosphorylated ATM

It is not known whether Aβ1-42 can induce the phosphorylation of ATM in cultured cortical neurons. We therefore analyzed the effect of Aβ1-42 on the expression level of phosphorylated ATM (pATM) at Ser1981, as an indicator of ATM activation, in cultured cortical neurons. Cultured cortical neurons were treated with 10 μM Aβ1-42 for 3 h or with 1 μM etoposide for 1 h as the positive control, and pATM expression level was determined by Western blot analysis using a specific antibody to ATM at Ser1981. We found an increase in pATM levels after the treatments with Aβ1-42 and etoposide (Figure 7A). To determine whether ATBF1 interacts with pATM, coimmunoprecipitation analysis was performed. Cultured cortical neurons were treated with 10 μM Aβ1-42 for 3 h or 1 μM etoposide for 1 h, and then subjected to immunoprecipitation with anti-ATBF1 antibody-conjugated Protein G beads followed by immunoblotting with the anti-pATM antibody. As shown in Figure 7B, ATBF1 interacted with pATM after treatment with Aβ1-42 or etoposide. Our findings suggest that ATBF1 expression was enhanced by Aβ1-42 and DNA-damaging drugs (etoposide and homocysteine) and increased the expression level of ATBF1, which in turn activated ATM signaling responsible for neuronal death through the binding of ATBF1 to pATM.

ATM was required for ATBF1 to activate the p21 promoter

To determine the functional relationship between ATBF1 and ATM, we carried out p21 (Waf1/Cip1) promoter assay using ATM (+/+) and ATM (-/-) human fibroblast cells. ATM has been shown to play a role in the induction of DNA double strand breaks to arrest the cell cycle via activation of p53, and ATBF1 activates the p21 promoter in collaboration with p53 [27]. As shown in Figure 8, irradiation with X-ray increased the p21 promoter activity in ATM (+/+) cells, but not in ATM (-/-) cells, which is consistent with a previous finding that p21 expression is not changed in ATM (-/-) cells treated with the DNA-damaging drug etoposide [34]. Overexpression of ATBF1 increased the p21 promoter activity in ATM (+/+) cells, but not in ATM (-/-) cells. The combination of X-ray irradiation and overexpression of ATBF1 in ATM (+/+) cells synergistically increased p21 promoter activity. Importantly, this effect of ATBF1 on p21 promoter activity was abolished in ATM (-/-) cells. This finding indicates that ATBF1 increases p21 promoter activity in an ATM-dependent manner.

Discussion

Recently, cell-cycle-related molecules have been implicated as required components in the mechanisms underlying neuronal death in response to injury, stroke, and neurodegenerative diseases including AD [35-38] and transgenic mouse models of AD [19,20]. We have previously reported that ATBF1 is highly expressed in postmitotic neurons but not in neural progenitor cells in the developing rat brain, and that its mRNA expression level is highest in the embryonic day 12.5 (E12.5) brain [25]. Moreover, the overexpression of ATBF1 induces cell cycle arrest in mouse neuroblastoma, human prostate cancer, and human breast cancer cell

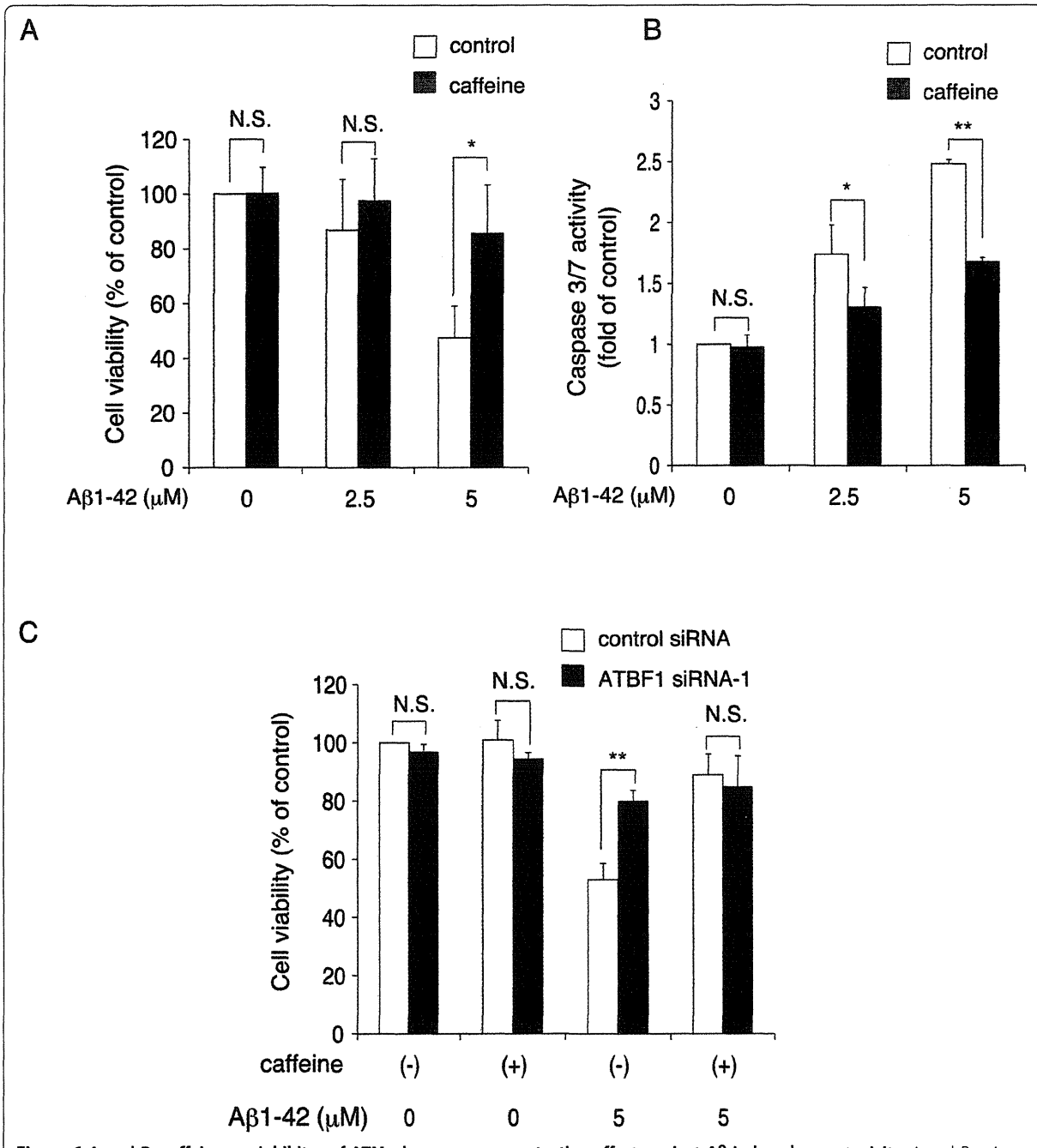

Figure 6 A and B, caffeine, an inhibitor of ATM, shows a neuroprotective effect against Aβ-induced neurotoxicity. A and B, primary cortical neurons were seeded at a density of 1×10^6 cells/ml in poly-d-lysine-coated 96-well plates. Three days after plating, cells were pretreated with 10 μM caffeine for 1 h, and subsequently treated for 16 h with 0, 2.5, or 5 μM Aβ1-42. Cell viability was determined using a CellTiter-Glo luminescent cell viability assay kit (A), and caspase-3/7 activity was determined using a Caspase-Glo™ 3/7 assay kit (B). C, after transfection as described in Fig 3B, cells were pretreated for 1 h with or without 10 μM caffeine, and then cells were further incubated with or without 5 μM Aβ1-42 for 16 h. Cell viability was determined using a CellTiter-Glo luminescent cell viability assay kit. All the values are presented as the mean ± SEM of three independent experiments. *$p < 0.05$, **$p < 0.01$ *vs* control siRNA. N.S., not significant, as determined by one-way ANOVA followed by Duncan's test.

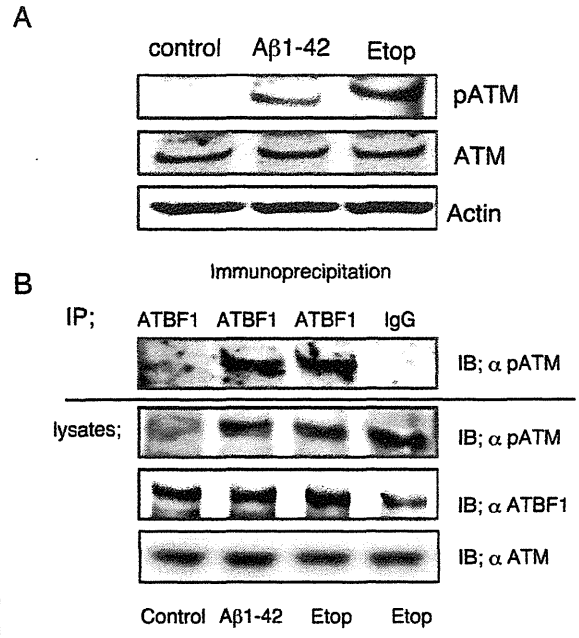

Figure 7 A, phosphorylation of ATM after treatment of primary cortical neurons with Aβ1-42 or etoposide. Primary cortical neurons were treated for 1 h with 10 μM Aβ1-42 or with 1 μM etoposide (Etop). The cells were lysed, and the protein expression levels of pATM, ATM, and actin were determined by Western blot analysis using the anti-pATM, anti-ATM, and anti-actin antibodies. B, ATBF1 interacts with pATM after treatment with Aβ1-42 or etoposide. Cultured cortical neurons were treated as described in A, cell lysates were immunoprecipitated with the anti-ATBF1 antibody. The immunoprecipitated complex was then subjected to immunoblotting with the anti-pATM at Ser1891 antibody. Typical bands representative of three independent experiments with similar results are shown.

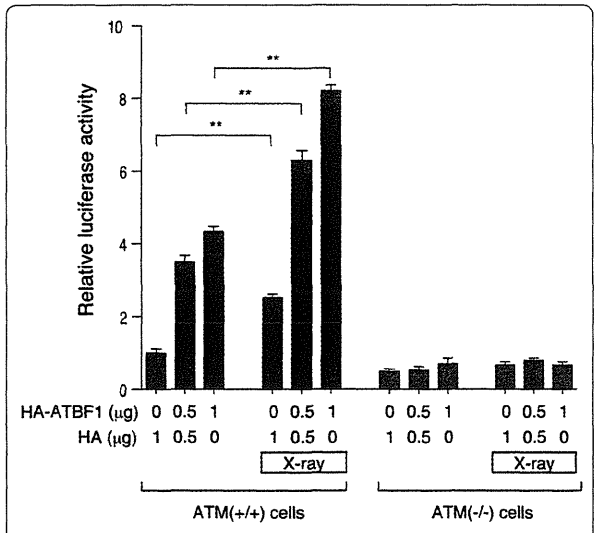

Figure 8 Effect of ATBF1 on activation of p21 promoter in X-ray-irradiated ATM (+/+) and ATM (-/-) cells. ATM (+/+) and ATM (-/-) cells were transfected with p21 promoter-luciferase, pRL-TK-luciferase (as an internal control), and an indicated dose of HA-ATBF1 vector or pCI-HA vector as a control. After 24 h, cells were irradiated with a 2.5 Gy X-ray, and then luciferase activity was measured after 12 h. All the values are presented as the mean ± SEM of three independent experiments. $^{**}p < 0.01$ *vs* not irradiated. N.S., not significant, as determined by Mann-Whitney *U*-test with Bonferroni Correction.

lines [25,28,29]. These findings suggest that ATBF1 may play critical roles in cell cycle arrest and proliferation. In the present study, we found that the ATBF1 expression level in the brains of 17-month-old wild-type mice decreased compared with that in the brains of 10-month-old wild-type mice. This finding is consistent with our previous finding that ATBF1 mRNA expression level gradually decreases with increasing age in the rat brain [25]. However, ATBF1 expression was up-regulated in the brains of 17-month-old Tg2576 mice compared with that in the brains of age-matched wild-type mice. In Tg2576 mice, diffuse plaques appear after 12 months, and their amount gradually increases with age [30]. Therefore, we considered that the increase in ATBF1 expression level was due to Aβ, and we found that the treatment with Aβ1-42 significantly increased the expression levels of ATBF1 mRNA and protein in cultured rat cortical neurons. The increase in ATBF1 expression level in the brains of 17-month-old Tg2576 mice could be triggered by the accumulation of extracellular Aβ similar to the Aβ-mediated increase in ATBF1 expression level observed in cultured cortical neurons. In addition, the reason why ATBF1 remains increased in 17-month-old Tg2576 mice could be that Aβ induces neurons to re-enter the cell cycle and ATBF1 prevents this process from occurring.

Aβ induces oxidative DNA damage. A previous study showed that the expression level of ATBF1 is increased in gastric cancer cells treated with mitomycin-C, which can induce DNA damage in many cell types [31]. This suggests that DNA damage might increase ATBF1 expression level. We, therefore, also examined whether treatment with DNA-damaging drugs, namely, etoposide and homocysteine, affects ATBF1 expression. Here, we found that these DNA-damaging drugs significantly increased the expression levels of ATBF1 mRNA and protein in cultured rat cortical neurons. These findings suggest that the up-regulated ATBF1 expression observed in our *in vivo* and *in vitro* experiments could be due to DNA damage induced by Aβ.

It has been reported that the consequences of DNA damage are the expression of cell-cycle-related proteins [22,39,40] and activation of the family of phosphatidylinositol-3 (PI3)-kinases that include the ATM protein, which is involved in the regulation of cell cycle and apoptosis by the phosphorylation of many downstream

substrates [41-43]. Therefore, one possibility is that ATM could constitute a common pathway activated in neuronal apoptosis after DNA damage. Recently, we have found that ATM induces ATBF1 expression during retinoicacid-induced neuronal differentiation of P19 cells by the activation and binding of CREB to a CRE consensus site located in the ATBF1 promoter (unpublished data). It has also been reported that the ATBF1 gene is one of the target genes of ATM that phosphorylates ATBF1 at Ser1180 [26]. These observations suggest that the activation of ATM highly correlates with the function and expression of ATBF1 as a gene regulatory factor. In this study, we observed that treatment with Aβ1-42 and etoposide rapidly posphorylates ATM at Ser 1981, and that ATBF1 interacts with pATM in cultured cortical neurons. Taken together, ATM activation induced by Aβ and DNA-damaging drugs may induce ATBF1 expression.

In this study, we also examined the effect of ATBF1 on neuronal death and apoptosis induced by Aβ1-42, etoposide, and homocysteine in cultured cortical neurons, and we found that the knockdown of ATBF1 by ATBF1 siRNA transfection significantly reduced the extent of cell death and apoptosis induced by Aβ1-42, etoposide, homocysteine. In addition, the knockdown of ATBF1 attenuated the activation of caspase-3/7. These findings suggest that the increased ATBF1 expression level may mediate apoptotic function in cultured cortical neurons against Aβ1-42-induced neurotoxicity. It has been reported that Aβ and DNA-damaging drugs induce the expression and activation of p53 which plays an important role in promoting apoptosis in cultured neurons [22,44]. Therefore, the increased ATBF1 expression level might simultaneously activate p53 to promote cell death, because ATBF1 interacts with p53 [27]. We also found in this study that ATBF1-mediated neuronal death is dependent on ATM signals because the blockage of ATM by treatment with ATM inhibitors, caffeine and KU55933, abolished ATBF1 functions in neuronal death. This finding is in agreement with our previous finding that caffeine treatment inhibits the translocalization of ATBF1 to the nucleus in P19 cells [25]. Further studies are necessary to characterize the role of ATBF1 in AD pathogenesis such as whether ATBF1 expression is altered in the AD brain.

Conclusions

In conclusion, the increase in ATBF1 expression level observed in the brain of 17-month-old Tg2576 mice compared with age-matched wild-type mice could be caused by DNA damage induced by Aβ1-42, which in turn activates the ATM signaling responsible for neuronal death, indicating that ATBF1 plays an important role in neuronal death in response to Aβ1-42, etoposide, and homocystein, and it may be a useful target in the development of drugs to suppress the neuronal death induced by Aβ1-42.

Methods

Tg2576 mice

Female Tg2576 mice, an animal model of amyloid deposition, overexpressing human APP695 with the Swedish mutation K670N/M671, were obtained from Taconic (Germantown, NY). All the experiments were performed in accordance with the Guidelines for Animal Experiments of the Animal Experimentation Committee of the National Center for Geriatrics and Gerontology.

Cell cultures

Cerebral cortical neurons were obtained from E17 Sprague-Dawley rats and cultured as described previously [45]. Briefly, embryonic brains were dissected, stripped of meninges, and minced with forceps. The minced tissue was incubated in 0.25% trypsin and 2 mg/ml DNase I in phosphate-buffered saline (PBS) at 37°C for 15 min. The fragments were then dissociated into single cells by pipetting. The dissociated cells were suspended in DMEM/F-12 medium (50:50%) containing N_2 supplements and 7.5% bovine albumin fraction V, and plated onto poly-d-lysine-coated 60 mm dishes at a density of 1×10^6/ml. These cells were used on day 4 of plating for further experiments. The immortalized fibroblast cell line AT22IJE-T was originally established from primary ataxia-telangiectasia (A-T) patient fibroblasts [46]. The cells were transfected with either the pEBS7 or pEGS7-YZ ATM vector to obtain AT22IJE-T/pEBS7 (ATM -/-) and AT22IJE-T/YZ5 (ATM +/+) cells, respectively [47]. Cells were maintained in DMEM containing 15% fetal bovine serum (FBS), 2 mM glutamine, 100 μg/ml hygromycin B, 100 U/ml penicillin, and 0.1 mg/ml streptomycin.

RNA extraction and real-time PCR

Total RNA was isolated from primary cortical neurons using an RNeasy plus mini kit (Qiagen, Valencia, CA) following the manufacturer's instructions. Reverse transcription was performed using 1 μg of total RNA using a PrimeScript RT reagent kit (Takara, Tokyo, Japan). Real-time PCR was carried out using the SYBR Premix Ex Taq system and Thermal Cycler Dice Real-Time system (Takara). The expression of the ATBF1 gene was normalized with the corresponding amount of actin mRNA using the comparative threshold cycle method following the manufacturer's protocols. Amplification was performed using the following primers (sense and antisense): ATBF1 (5'-CAAAACTTCTGCTGCCCTTC-3' and 5'-GGCTTGTCTCAAGGTGC-TTC-3') and actin (5'-CATCCGTAAAGACCTCTATGCCAAC-3' and 5'-ATGGA-GCCACCGATCCACA-3').

Aβ1–42 treatment

The synthetic Aβ1-42 peptide was purchased from Peptide Institute (Osaka, Japan), dissolved in 0.1% NH_3 to the final concentration of 1 mM, and stored at -80°C until use. To confirm the state of the Aβ1-42 peptide, we performed Western blot analysis. Briefly, a stored Aβ1-42 peptide was subjected to 16% Tris-Tricine Gel (Invitrogen) electrophoresis and transferred to polyvinylidene difluoride (PVDF) membranes (Millipore, Billerica, MA). These membranes were incubated with a primary antibody against mouse monoclonal human Aβ (6E10; Covance, Emeyryville, CA). For detection, the membrane was incubated with a horseradish-peroxidase-conjugated Ig anti-mouse antibody. Immunoreaction signals were visualized with ECL™ or ECL Plus™ Western blotting detection reagent (GE Healthcare, Piscataway, NJ) and exposed to the LAS-3000 Mini Bio-imaging Analyzer System (FUJIFILM Co., Tokyo, Japan).

Western blot analysis

The cells were washed with PBS and homogenized in lysis buffer (10 mM Tris-HCl (pH 7.4), 150 mM NaCl, 1 mM EDTA, 1% Triton X-100) containing a protease inhibitor cocktail (Roche, Mannheim, Germany). The homogenates were rocked at 4°C for 30 min and centrifuged at 13,000 × *g* at 4°C for 30 min to remove cell debris. The resulting supernatant was collected and protein concentration was determined using a BCA protein assay kit (Pierce, Rockford, IL). Equal amounts of protein were subjected to 7.5% or 5-20% gradient SDS polyacrylamide gel electrophoresis, and separated products were transferred to PVDF membranes. These membranes were then blocked with 5% skim milk in 10 mM Tris-HCl (pH 7.5), 150 mM NaCl, and 0.1% Tween 20 for 1 h at room temperature or overnight at 4°C. These membranes were incubated with primary antibodies, namely, the anti-ATBF1 (AT-6) antibody (1:1000; MBL, Nagoya, Japan), anti-p53 antibody (1:1000; Cell Signaling, Cambridge, UK), anti-ATM antibody (1:1000; Gene Tex, Irvine, CA), anti-ATM kinase pS1981 antibody (1:1000; Rockland, Gilbertsville, PA), or anti-actin antibody (1:2,000; Sigma, Saint Louis, MO). The membranes were washed, and then incubated with the appropriate secondary antibody conjugated to horseradish peroxidase. Immunoreaction signals were visualized with ECL™ or ECL Plus™ Western blotting detection reagent and exposed to the LAS-3000 Mini Bio-imaging Analyzer System. Signal intensity was determined using MultiGauge software (FUJIFILM).

RNA interference

Endogenous ATBF1 was knocked down using predesigned Stealth™siRNA against ATBF1 (ATBF1 siRNA) and Stealth siRNA negative control (control siRNA) from Invitrogen (Carlsbad, CA). The ATBF1 siRNAs sequences are as follows: ATBF1-siRNA-1 sense (5'-UAC ACU GGU CAG ACC ACU GUC CUU G-3') and antisense (5'-CAA GGA CAG UGG UCU GAC CAG UGU -3'). ATBF1-siRNA-2 sense (5'- UAC ACU GGU CAG ACC ACU GUC CUU G-3') and antisense (5'-TAC ACT GGT CAG ACC ACT GTC CTT G-3'). The primary cultured neurons were transiently transfected with 50 nM ATBF1 siRNA or with control siRNA using Lipofectamine RNAiMAX (Invitrogen) in accordance with the manufacturer's instructions. The knockdown effects were examined after 48 h of incubation. The cultures were then processed for Western blot analysis, cell viability analysis and terminal deoxynucleotidyl transferase-mediated dUTP nick-end labeling (TUNEL) assay 16 h after Aβ1-42 treatment.

Cell viability analysis

Neuronal viability was evaluated by CellTiter-Glo luminescent cell viability assay (Promega, Madison, WI), which is a method to determine the number of viable cells in culture based on the quantitation of ATP present, which indicates the presence of metabolically active cells. Briefly, primary cortical neurons were seeded onto poly-d-lysine-coated 96-well plates, and incubated for 72 h. For the ATBF1 knockdown experiment, the cells were transfected with ATBF1 siRNA or with control siRNA for 48 h as described above, cells were then treated with Aβ1–42, etoposide, or homocysteine at indicated doses for 16 h. After treatment, a volume of CellTiter-Glo Reagent was added to each well equal to the volume of cell culture medium. Then, the contents were mixed for 2 min on a shaker to induce cell lysis and the plates were incubated at room temperature for 10 min in the dark. Cellular luminescence intensity was measured using a GLOMAX 96-microplate luminometer (Promega).

Plasmid constructs

The ATBF1 expression vector of an 11 kb full-length human cDNA [23] was inserted into the pCI vector (Promega) with an HA-tagged sequence at the 5'-terminus of the inserted sequence (HA-ATBF1) [25]. The 2.4 kb fragment upstream from the TATA-box of the human p21 (Waf1/Cip1) genomic fragment was subcloned into the basic luciferase reporter pGV-B vector (Toyo Ink Co., Ltd., Tokyo, Japan) [48].

TUNEL assay

Apoptosis was assessed by TUNEL using an ApopTag Fluorescein Direct In Situ Apoptosis Detection kit in accordance with the manufacturer's instructions (Chemicon, Temecula, CA). Briefly, cells were fixed with 1% paraformaldehyde in PBS for 10 min at room temperature

and permeabilized in EtOH:acetic acid (2:1) for 5 min at -20°C. Cells were then washed with PBS. Fluorescein-conjugated nucleotide and TdT enzyme were added to the cells, which were then incubated for 1 h at 37°C. Nuclei were stained with DAPI. Images were obtained using an AX70 fluorescence microscope (Olympus). The percentage of apoptotic cells was determined as the ratio of the number of DAPI-TUNEL-double-positive cells with respect to the total number of DAPI-positive cells. For the overexpression of ATBF1 in cultured cortical neurons, the neurons were transiently transfected with 0.5 μg HA-ATBF1 using FuGENE HD (Roche) in accordance with the manufacturer's instructions. Twenty-four hours after transfection, TUNEL was performed as described in above. After TUNEL, the neurons were incubated with the primary antibody against HA-tag (MBL) for 1 h at RT. The secondary antibody was Alexa-594-conjugated goat anti-rabbit IgG (Molecular Probes). Images were obtained using an AX70 fluorescence microscope (Olympus).

Caspase-3/7 activity assay

Caspase-3/7 activity was assayed using a Caspase-Glo™ 3/7 assay kit (Promega), in accordence with the manufacturer's instructions. Briefly, primary cortical neurons were seeded on 96-well plates at a density of 1×10^6 cells/ml. After 3 days, the cells were treated with Aβ1-42 or DNA-damaging drugs. Caspase-Glo™ 3/7 reagent was then added to each well, and the plates were incubated at room temperature for 1 h. Cellular luminescence was measured using a GLOMAX 96-microplate luminometer (Promega).

Immunoprecipitation

Primary cortical neurons were grown in 10 cm dishes. After reaching 50-70% confluence, the cells were treated with 10 μM Aβ1–42 or 1 μM etoposide for an indicated time. After incubation, the cells were washed twice with PBS, lysed in 1 ml of lysis buffer (10 mM Tris-HCl (pH 7.4), 150 mM NaCl, 1 mM EDTA, 1% Triton X-100, 50 mM NaF, and 100 uM sodium orthovanadate) containing protease inhibitor cocktail, and centrifuged at 13,000 × *g* at 4°C for 20 min. The resulting supernatant was immunoprecipitated overnight with a specific antibody against ATBF1 (AT-6) in the presence of protein G beads (Pierce) at 4°C. The immune complexes were washed four times with lysis buffer. The samples were subjected to 5-20% gradient SDS polyacrylamide ge electrophoresis, and separated products were transferred to a PVDF membrane and subjected to immunoblotting with a specific antibody against phosphorylated-ATM (pATM) at Ser 1981.

X-ray irradiation and p21 promoter assay

ATM (+/+) and ATM (-/-) cells were transfected with p21 promoter-luciferase, pRL-TK-luciferase (as an internal control), and an indicated dose of the HA-ATBF1 vector or pCI-HA vector as the control using Lipofectamine 2000 (Invitrogen) in accordance with manufacturer's instructions. After 24 h, the cells were irradiated with X-ray at 2.5 Gy using a Softex M-80WE X-ray generator (SOFTEX, Japan) operating at 80 kv and 10 mA for 25 min with a copper shield. Nonirradiated dells were used as control. After 12 h, luciferase activity was measured using the Dual Luciferase Reporter Assay system (Promega) in accordance with the manufacturer's instructions.

Statistical analysis

Statistical analysis was performed using a statistical package, GraphPad prism software (GraphPad Software, San Diego, CA). All values are presented as the mean ± SEM of at least three independent experiments.

Additional material

Additional file 1: Western blot analysis of Aβ1-42 peptide used in our experiments. The stored Aβ1-42 peptide was diluted with culture medium to the final concentration of 5 μM, and then 0.5 (lane 1), 1 (lane 2), or 2.5 μl (lane 3) was loaded to 16% Tris-Tricine gel and probed with the monoclonal antibody 6E10 (recognizing residues 1-17 of Aβ).

Additional file 2: Effect of another ATBF1 siRNA (ATBF1 siRNA-2) on the viability of primary cortical neurons upon treatment with Aβ1-42. A, Primary cortical neurons were transfected with ATBF1 siRNA-2 or control siRNA for 48 h. After transfection, the cells were then incubated in the presence or absence of 5 μM Aβ1-42 for 16 h. The expression levels of ATBF1 and actin were determined by Western blot analysis using the anti-ATBF1 and anti-actin antibodies. B, After transfection as described in Figure 3B, the cells were treated with or without 5 μM Aβ1-42 for 16 h. Cell viability was determined using a CellTiter-Glo luminescent cell viability assay kit and is shown as a percentage of surviving cells. All the values are presented as the mean ± SEM of three independent experiments. *$p < 0.01$ *vs* control siRNA treatment. N.S., not significant, as determined by Student's *t*-test.

Additional file 3: A, KU55933, a specific ATM inhibitor, shows a neuroprotective effect against Aβ 1-42-, etoposide-, and homocysteine-induced neurotoxicity. Primary cortical neurons were seeded at a density of 1×10^6 cells/ml in poly-d-lysine-coated 96-well plates. Three days after plating, cells were pretreated with 0, 1, 5, or 10 μM KU55933 for 1 h, and subsequently treated for 16 h with 5 μM Aβ1-42, 1 μM etoposide (Etop), or 250 μM homocysteine (Hom). Cell viability was determined using a CellTiter-Glo luminescent cell viability assay kit. B, after transfection as described in Figure 3B, cells were pretreated for 1 h with or without 1 μM KU55933, and then cells were further incubated with or without 5 μM Aβ1-42 for 16 h. Cell viability was determined using a CellTiter-Glo luminescent cell viability assay kit. All the values are presented as the mean ± SEM of three independent experiments. *$p < 0.001$ *vs* control siRNA. N.S., not significant, as determined by one-way ANOVA followed by Duncan's test.

Abbreviations

ATBF1: AT-motif binding factor-1; Aβ: Amyloid-β peptide; AD: Alzheimer's disease; APP: Amyloid precursor protein; PS: presenilin; APOE:

apoplipoprotein E; ATM: Ataxia-telangiectasia mutated; pATM: phosphorylated ATM; PI3K: phospatidylinositol-3 kinase; TUNEL: Terminal deoxynucleotidyl transferase-mediated dUTP nick-end labeling.

Acknowledgements
We thank Eri Arata for technical assistance in Western blot analysis. We thank Makoto Nakanishi for providing the p21 (Waf1/Cip1) promoter DNA fragment. This work was supported by a Grant-in-Aid for Scientific Research (C) from the Ministry of Education, Culture, Sports, Science and Technology of Japan (CGJ) and a grant from the Japan Health Sciences Foundation for the Research on Publicly Essential Drugs and Medical Devices (MM, KHC1104) and a grant from The Research Funding for Longevity Sciences (21-A11) from National Center for Geriatrics and Gerontology (NCGG) (CGJ and MM), Japan and a Grant-in-Aid from the Japan Science and Technology Agency (YM).

Author details
[1]Department of Alzheimer's Disease Research, Research Institute, National Center for Geriatrics and Gerontology (NCGG), 35, Morioka, Obu, Aichi 474-8511, Japan. [2]Department of Molecular Neurobiology, Graduate School of Medical Sciences, Nagoya City University, Nagoya, 467-8601, Japan. [3]Queensland Institute of Medical Research and University of Queensland Centre, for Clinical Research, Brisbane 4029, Queensland, Australia.

Authors' contributions
CGJ designed this study, carried out major parts of the experiments, and drafted the manuscript. KOU prepared primary cortical neurons. YM, TH, HH, and MJK carried out the experiments. KKK provided comments on the manuscript. MM participated in the design of the study and in drafting the manuscript.
All authors have read and approved the final manuscript

Competing interests
The authors declare that they have no competing interests.

Received: 22 October 2010 Accepted: 5 July 2011 Published: 5 July 2011

References

1. Selkoe DJ: **Alzheimer's disease: genes, proteins, and therapy.** *Physiol Rev* 2001, **81**:741-766.
2. Tanzi RE, Bertram L: **Twenty years of the Alzheimer's disease amyloid hypothesis: a genetic perspective.** *Cell* 2005, **120**:545-555.
3. Goate A, Chartier-Harlin MC, Mullan M, Brown J, Crawford F, Fidani L, Giuffra L, Haynes A, Irving N, James L, *et al*: **Segregation of a missense mutation in the amyloid precursor protein gene with familial Alzheimer's disease.** *Nature* 1991, **349**:704-706.
4. Sherrington R, Rogaev EI, Liang Y, Rogaeva EA, Levesque G, Ikeda M, Chi H, Lin C, Li G, Holman K, *et al*: **Cloning of a gene bearing missense mutations in early-onset familial Alzheimer's disease.** *Nature* 1995, **375**:754-760.
5. Rogaev EI, Sherrington R, Rogaeva EA, Levesque G, Ikeda M, Liang Y, Chi H, Lin C, Holman K, Tsuda T, *et al*: **Familial Alzheimer's disease in kindreds with missense mutations in a gene on chromosome 1 related to the Alzheimer's disease type 3 gene.** *Nature* 1995, **376**:775-778.
6. Saunders AM, Strittmatter WJ, Schmechel D, George-Hyslop PH, Pericak-Vance MA, Joo SH, Rosi BL, Gusella JF, Crapper-MacLachlan DR, Alberts MJ, *et al*: **Association of apolipoprotein E allele epsilon 4 with late-onset familial and sporadic Alzheimer's disease.** *Neurology* 1993, **43**:1467-1472.
7. Frautschy SA, Baird A, Cole GM: **Effects of injected Alzheimer beta-amyloid cores in rat brain.** *Proc Natl Acad Sci USA* 1991, **88**:8362-8366.
8. Kowall NW, Beal MF, Busciglio J, Duffy LK, Yankner BA: **An in vivo model for the neurodegenerative effects of beta amyloid and protection by substance P.** *Proc Natl Acad Sci USA* 1991, **88**:7247-7251.
9. Behl C, Davis JB, Klier FG, Schubert D: **Amyloid beta peptide induces necrosis rather than apoptosis.** *Brain Res* 1994, **645**:253-264.
10. Loo DT, Copani A, Pike CJ, Whittemore ER, Walencewicz AJ, Cotman CW: **Apoptosis is induced by beta-amyloid in cultured central nervous system neurons.** *Proc Natl Acad Sci USA* 1993, **90**:7951-7955.
11. Busser J, Geldmacher DS, Herrup K: **Ectopic cell cycle proteins predict the sites of neuronal cell death in Alzheimer's disease brain.** *J Neurosci* 1998, **18**:2801-2807.
12. Liu WK, Williams RT, Hall FL, Dickson DW, Yen SH: **Detection of a Cdc2-related kinase associated with Alzheimer paired helical filaments.** *Am J Pathol* 1995, **146**:228-238.
13. McShea A, Harris PL, Webster KR, Wahl AF, Smith MA: **Abnormal expression of the cell cycle regulators P16 and CDK4 in Alzheimer's disease.** *Am J Pathol* 1997, **150**:1933-1939.
14. Vincent I, Jicha G, Rosado M, Dickson DW: **Aberrant expression of mitotic cdc2/cyclin B1 kinase in degenerating neurons of Alzheimer's disease brain.** *J Neurosci* 1997, **17**:3588-3598.
15. Copani A, Uberti D, Sortino MA, Bruno V, Nicoletti F, Memo M: **Activation of cell-cycle-associated proteins in neuronal death: a mandatory or dispensable path?** *Trends Neurosci* 2001, 25-31.
16. Ogawa O, Lee HG, Zhu X, Raina A, Harris PL, Castellani RJ, Perry G, Smith MA: **Increased p27, an essential component of cell cycle control, in Alzheimer's disease.** *Aging Cell* 2003, **2**:105-110.
17. Evans TA, Raina AK, Delacourte A, Aprelikova O, Lee HG, Zhu X, Perry G, Smith MA: **BRCA1 may modulate neuronal cell cycle re-entry in Alzheimer disease.** *Int J Med Sci* 2007, 140-145.
18. Cenini G, Sultana R, Memo M, Butterfield DA: **Effects of oxidative and nitrosative stress in brain on p53 proapoptotic protein in amnestic mild cognitive impairment and Alzheimer disease.** *Free Radic Biol Med* 2008, **45**:81-85.
19. Hsiao K, Chapman P, Nilsen S, Eckman C, Harigaya Y, Younkin S, Yang F, Cole G: **Correlative memory deficits, Abeta elevation, and amyloid plaques in transgenic mice.** *Science* 1996, **274**:99-102.
20. Yang Y, Varvel NH, Lamb BT, Herrup K: **Ectopic cell cycle events link human Alzheimer's disease and amyloid precursor protein transgenic mouse models.** *J Neurosci* 2006, **26**:775-784.
21. Lopes JP, Oliveira CR, Agostinho P: **Cdk5 acts as a mediator of neuronal cell cycle re-entry triggered by amyloid-beta and prion peptides.** *Cell Cycle* 2009, **8**:97-104.
22. Wersto RP, Cardozo-Pelaez F, Smilenov L, Chan SL, Chrest FJ, Emokpae R Jr, Gorospe M, Mattson MP: **Cell cycle activation linked to neuronal cell death initiated by DNA damage.** *Neuron* 2004, **41**:549-561.
23. Miura Y, Tam T, Ido A, Morinaga T, Miki T, Hashimoto T, Tamaoki T: **Cloning and characterization of an ATBF1 isoform that expresses in a neuronal differentiation-dependent manner.** *J Biol Chem* 1995, **270**:26840-26848.
24. Morinaga T, Yasuda H, Hashimoto T, Higashio K, Tamaoki T: **A human alpha-fetoprotein enhancer-binding protein, ATBF1, contains four homeodomains and seventeen zinc fingers.** *Mol Cell Biol* 1991, **11**:6041-6049.
25. Jung CG, Kim HJ, Kawaguchi M, Khanna KK, Hida H, Asai K, Nishino H, Miura Y: **Homeotic factor ATBF1 induces the cell cycle arrest associated with neuronal differentiation.** *Development* 2005, **132**:5137-5145.
26. Matsuoka S, Ballif BA, Smogorzewska A, McDonald ER, Hurov KE, Luo J, Bakalarski CE, Zhao Z, Solimini N, Lerenthal Y, *et al*: **ATM and ATR substrate analysis reveals extensive protein networks responsive to DNA damage.** *Science* 2007, **316**:1160-1166.
27. Miura Y, Kataoka H, Joh T, Tada T, Asai K, Nakanishi M, Okada N, Okada H: **Susceptibility to killer T cells of gastric cancer cells enhanced by Mitomycin-C involves induction of ATBF1 and activation of p21 (Waf1/Cip1) promoter.** *Microbiol Immunol* 2004, **48**:137-145.
28. Sun X, Frierson HF, Chen C, Li C, Ran Q, Otto KB, Cantarel BL, Vessella RL, Gao AC, Petros J, *et al*: **Frequent somatic mutations of the transcription factor ATBF1 in human prostate cancer.** *Nat Genet* 2005, **37**:407-412.
29. Dong XY, Sun X, Guo P, Li Q, Sasahara M, Ishii Y, Dong JT: **ATBF1 inhibits ER function by selectively competing with AIB1 for binding to ER in ER-positive breast cancer cells.** *J Biol Chem* **285(43)**:32801-9.
30. Kawarabayashi T, Younkin LH, Saido TC, Shoji M, Ashe KH, Younkin SG: **Age-dependent changes in brain, CSF, and plasma amyloid (beta) protein in the Tg2576 transgenic mouse model of Alzheimer's disease.** *J Neurosci* 2001, **21**:372-381.
31. Kamiguchi Y, Tateno H: **Radiation- and chemical-induced structural chromosome aberrations in human spermatozoa.** *Mutat Res* 2002, **504**:183-191.
32. Roth KA: **Caspases, apoptosis, and Alzheimer disease: causation, correlation, and confusion.** *J Neuropathol Exp Neurol* 2001, **60**:829-838.
33. Bryant HE, Helleday T: **Inhibition of poly (ADP-ribose) polymerase activates ATM which is required for subsequent homologous recombination repair.** *Nucleic Acids Res* 2006, **34**:1685-1691.

34. Tang D, Wu D, Hirao A, Lahti JM, Liu L, Mazza B, Kidd VJ, Mak TW, Ingram AJ: **ERK activation mediates cell cycle arrest and apoptosis after DNA damage independently of p53.** *J Biol Chem* 2002, **277**:12710-12717.
35. Greene LA, Biswas SC, Liu DX: **Cell cycle molecules and vertebrate neuron death: E2F at the hub.** *Cell Death Differ* 2004, **11**:49-60.
36. Herrup K, Neve R, Ackerman SL, Copani A: **Divide and die: cell cycle events as triggers of nerve cell death.** *J Neurosci* 2004, **24**:9232-9239.
37. Nunomura A, Moreira PI, Lee HG, Zhu X, Castellani RJ, Smith MA, Perry G: **Neuronal death and survival under oxidative stress in Alzheimer and Parkinson diseases.** *CNS Neurol Disord Drug Targets* 2007, **6**:411-423.
38. Rashidian J, Iyirhiaro GO, Park DS: **Cell cycle machinery and stroke.** *Biochim Biophys Acta* 2007, **1772**:484-493.
39. Keramaris E, Hirao A, Slack RS, Mak TW, Park DS: **Ataxia telangiectasia-mutated protein can regulate p53 and neuronal death independent of Chk2 in response to DNA damage.** *J Biol Chem* 2003, **278**:37782-37789.
40. Krantic S, Mechawar N, Reix S, Quirion R: **Molecular basis of programmed cell death involved in neurodegeneration.** *Trends Neurosci* 2005, **28**:670-676.
41. Kurz EU, Lees-Miller SP: **DNA damage-induced activation of ATM and ATM-dependent signaling pathways.** *DNA Repair (Amst)* 2004, **3**:889-900.
42. Ljungman M: **Activation of DNA damage signaling.** *Mutat Res* 2005, **577**:203-216.
43. McKinnon PJ: **Ataxia telangiectasia: new neurons and ATM.** *Trends Mol Med* 2001, **7**:233-234.
44. Ubertí D, Ferrari Toninelli G, Memo M: **Involvement of DNA damage and repair systems in neurodegenerative process.** *Toxicol Lett* 2003, **139**:99-105.
45. Michikawa M, Gong JS, Fan QW, Sawamura N, Yanagisawa K: **A novel action of alzheimer's amyloid beta-protein (Abeta): oligomeric Abeta promotes lipid release.** *J Neurosci* 2001, **21**:7226-7235.
46. Ziv Y, Jaspers NG, Etkin S, Danieli T, Trakhtenbrot L, Amiel A, Ravia Y, Shiloh Y: **Cellular and molecular characteristics of an immortalized ataxia-telangiectasia (group AB) cell line.** *Cancer Res* 1989, **49**:2495-2501.
47. Ziv Y, Bar-Shira A, Pecker I, Russell P, Jorgensen TJ, Tsarfati I, Shiloh Y: **Recombinant ATM protein complements the cellular A-T phenotype.** *Oncogene* 1997, **15**:159-167.
48. Nojiri S, Joh T, Miura Y, Sakata N, Nomura T, Nakao H, Sobue S, Ohara H, Asai K, Ito M: **ATBF1 enhances the suppression of STAT3 signaling by interaction with PIAS3.** *Biochem Biophys Res Commun* 2004, **314**:97-103.

doi:10.1186/1750-1326-6-47
Cite this article as: Jung *et al.*: Beta-amyloid increases the expression level of ATBF1 responsible for death in cultured cortical neurons. *Molecular Neurodegeneration* 2011 **6**:47.

The American Journal of Pathology, Vol. 180, No. 5, May 2012

DOI: 10.1016/j.ajpath.2012.01.015

Matrix Pathobiology

Heparan Sulfate Subdomains that are Degraded by Sulf Accumulate in Cerebral Amyloid ß Plaques of Alzheimer's Disease

Evidence from Mouse Models and Patients

Tomomi Hosono-Fukao,* Shiori Ohtake-Niimi,*† Hitomi Hoshino,* Markus Britschgi,‡ Hiroyasu Akatsu,§ Md. Motarab Hossain,* Kazuchika Nishitsuji,¶ Toin H. van Kuppevelt,‖ Koji Kimata,** Makoto Michikawa,¶ Tony Wyss-Coray,‡ and Kenji Uchimura*†¶

From the Section of Pathophysiology and Neurobiology, Department of Alzheimer's Disease Research,¶ National Center for Geriatrics and Gerontology, Obu, Japan; the Department of Biochemistry,† Graduate School of Medicine, Nagoya University, Nagoya, Japan; the Department of Neurology and Neurological Sciences,‡ Stanford University School of Medicine, Stanford, California; the Choju Medical Institute,§ Fukushimura Hospital, Toyohashi, Japan; the Department of Biochemistry,‖ Radboud University Nijmegen Medical Center, Nijmegen, The Netherlands; and the Research Complex for the Medicine Frontiers,** Aichi Medical University, Nagakute, Japan*

Alzheimer's disease (AD) is characterized by extracellular cerebral accumulation of amyloid β peptide (Aβ). Heparan sulfate (HS) is a glycosaminoglycan that is abundant in the extracellular space. The state of sulfation within the HS chain influences its ability to interact with a variety of proteins. Highly sulfated domains within HS are crucial for Aβ aggregation *in vitro*. Here, we investigated the expression of the sulfated domains and HS disaccharide composition in the brains of Tg2576, J20, and T41 transgenic AD mouse models, and patients with AD. RB4CD12, a phage display antibody, recognizes highly sulfated domains of HS. The RB4CD12 epitope is abundant in the basement membrane of brain vessels under physiological conditions. In the cortex and hippocampus of the mice and patients with AD, RB4CD12 strongly stained both diffuse and neuritic amyloid plaques. Interestingly, RB4CD12 also stained the intracellular granules of certain hippocampal neurons in AD brains. Disaccharide compositions in vessel-enriched and nonvasculature fractions of Tg2576 mice and AD patients were found to be comparable to those of non-transgenic and non-demented controls, respectively. The RB4CD12 epitope in amyloid plaques was substantially degraded *ex vivo* by Sulf-1 and Sulf-2, extracellular HS endosulfatases. These results indicate that formation of highly sulfated HS domains may be upregulated in conjunction with AD pathogenesis, and that these domains can be enzymatically remodeled in AD brains. *(Am J Pathol 2012, 180: 2056–2067; DOI: 10.1016/j.ajpath.2012.01.015)*

Heparan sulfate (HS) is a linear polysaccharide that exists in large quantities in the extracellular space. One or more HS chains are covalently bound to a core protein comprising heparan sulfate proteoglycan (HSPG).[1,2] HS chains and heparins, structural analogues of HS chains, are a family of glycosaminoglycans consisting of repeating disaccharide units of glucuronic/iduronic acid and glucosamine. Modification with sulfation as well as elongation of these disaccharides is enzymatic,[3] bestowing on the chains structural diversity.[4–6] HS contains highly

This work was supported by grants from the Japanese Health and Labour Sciences Research (Comprehensive Research on Aging and Health H19-001 and H22-007 to K.U., H20-007 to M.M.), Grants-in-Aid from the Ministry of Education, Science, Sports and Culture (22790303 to K.U. and JBBNNR, Comprehensive Brain Science Network to H.A.), and in part from the Sanofi-Aventis Science Foundation of Japan (to K.U.), the Naito Science Foundation (to K.U.), the Takeda Science Foundation (to K.U.), and the Daiko Foundation (to K.U.).

Accepted for publication January 19, 2012.

Present address of M.B., F. Hoffmann-La Roche Ltd, pRED, CNS Discovery, CH-4070, Basel, Switzerland.

Supplemental material for this article can be found on *http://ajp.amjpathol.org* or at doi: 10.1016/j.ajpath.2012.01.015.

Address reprint requests to Kenji Uchimura, Ph.D., Department of Biochemistry, Graduate School of Medicine, Nagoya University, 65 Tsurumai, Showa, Nagoya, Aichi, 466-8550 Japan. E-mail: arumihcu@med.nagoya-u.ac.jp.

sulfated domains and partially sulfated or non-sulfated domains, which are transitional.[3] Highly sulfated domains are formed by consecutive clusters of sulfated disaccharides. It has been shown that a trisulfated disaccharide structure [-iduronic acid(2S)-Glucosamine(NS,6S)-] occurs within highly sulfated domains. RB4CD12, a phage display anti-HS antibody, has been shown to recognize trisulfated disaccharide-containing HS subdomains[7–9] Trisulfated disaccharides are considered to be key elements in molecular interactions between HS/heparin and many ligands, including growth factors and morphogens.[1,10] Trisulfated disaccharides, as well as the RB4CD12 epitope, are degraded by extracellular sulfatases, Sulf-1, and Sulf-2.[8,11,12] In the brain, we have shown that the RB4CD12 HS domains are abundantly present in the vasculature[9] and that these domains can be degraded by the Sulfs *ex vivo*.[8] However, the roles of the RB4CD12 HS domains in pathological and physiological processes in brain vasculature are not known.

Alzheimer's disease (AD) is a progressive neurodegenerative disorder. One of the pathological hallmarks of AD is the presence of extracellular amyloid plaques in brain areas that are responsible for cognition and memory functions. The predominant composition of amyloid plaques is fibrils made of amyloid β peptide (Aβ). A great deal of biochemical and genetic evidence has indicated that aggregation and accumulation of Aβ in toxic forms within the extracellular space play a central role in AD pathogenesis. One of the authors previously reported that certain structures of HS chains exist in amyloid plaques of AD brains,[13] and that structural variation of HSPG correlates with amyloid plaque formation in the brains of AD patients.[14] HSPG is also known to facilitate cerebral amyloid deposition induced exogenously in a rat model *in vivo*.[15] Functional roles of HS and HSPG in AD pathology are proposed to be acceleration of Aβ fibril formation and protection of the fibril against microglial phagocytosis.[16] It was reported that the aggregation state of Aβ requires its binding properties to heparin.[17] Pathological correlations between the RB4CD12 HS domains, which are rich in heparin and AD have not been established. Here we present evidence that the RB4CD12 HS domains are accumulated in cerebral amyloid plaques of transgenic AD mouse models and patients with AD, and that these HS epitopes can be degraded by Sulf-1 and Sulf-2 *ex vivo*.

Materials and Methods

Materials

The RB4CD12 phage display-derived anti-heparan sulfate antibody was produced in a vesicular stomatitis virus (VSV)-tag version and purified as previously described.[7] Alternative nomenclature of RB4CD12 is HS3A8. The following materials were commercially obtained from the sources indicated. Heparinases (I, II and III), polyclonal rabbit anti-laminin antibody (Ab), horseradish peroxidase-conjugated monoclonal anti-VSV Ab, and Cy3-conjugated monoclonal anti-VSV Ab were from Sigma (St. Louis, MO); biotinylated monoclonal anti-amyloid β (N-terminus) Ab (82E1) was from IBL (Gunma, Japan); polyclonal rabbit anti-VSV Ab was from Bethyl Laboratories (Montgomery, TX); Cy2-conjugated goat anti-mouse IgG (H+L), Cy2-conjugated goat anti-rabbit IgG (H+L), Cy2-conjugated goat anti-rat IgG (H+L) Abs, and Cy2-conjugated streptavidin were from Jackson ImmunoResearch Laboratories (West Grove, PA); rabbit anti-Iba1 Ab was from Wako Pure Chemical Industries, Ltd. (Osaka, Japan); rabbit anti-glial fibrillary acidic protein and monoclonal anti-phospho-PHF-tau pThr231 (AT180) Abs were from Thermo Scientific (Rockford, IL); goat anti-mouse syndecan-3 Ab was from R&D Systems, Inc (Minneapolis, MN); rabbit anti-glypican-1 (M-95) Ab was from Santa Cruz Biotechnology, Inc (Santa Cruz, CA); polyclonal goat anti-rabbit IgG Nanogold, ϕ1.4 nm, was from Nanoprobes (Yaphank, NY); and horseradish peroxidase-conjugated goat anti-rabbit IgG was from Cell Signaling Technology, Inc. (Beverly, MA).

Animals

C57BL/6 mice were from Japan SLC Inc. (Hamamatsu, Japan). Heterozygotic transgenic mice that expressed the human amyloid precursor protein bearing the Swedish (K670N, M671L) mutation (Tg2576 strain),[18] the Swedish and Indiana (V717F) mutations (J20 strain),[19] or the Swedish and London (V717I) mutations (T41 strain)[20] were maintained in barrier facilities. Tg2576 mice were purchased from Taconic Farms, Inc., Hudson, NY. J20 mice were from the Jackson Laboratory (Bar Harbor, ME). The National Center of Geriatrics and Gerontology Institutional Animal Care and Use Committee approved the animal studies.

Human Postmortem Brain Tissues

Patients with sporadic AD received a pathological diagnosis according to the criteria of the Consortium to Establish a Registry for Alzheimer's Disease and the Braak stage. Non-demented controls were elderly patients who were age-matched and without significant neurological disorders. Patients were also cognitively evaluated by neuropsychological tests using the Mini-Mental State Examination and Hasegawa's dementia scale, which is commonly used in Japan. Entorhinal cortex and hippocampus postmortem tissue samples from neurologically unimpaired subjects (non-demented controls [NDCs]) and from subjects with AD were obtained under Committees on Human Research approval of National Center for Geriatrics and Gerontology and Choju Medical Institute of Fukushimura Hospital. Diagnosis of AD was confirmed by pathological and clinical criteria (Table 1). The incidence of vascular risk factors (eg, atherosclerosis, myocardial infarction, and so forth), the sex ratio, age, and the postmortem interval were comparable between NDC and AD (Table 1). Tissue was cut and frozen or fixed with formalin, and then embedded with paraffin. Frozen tissues were subjected to structural analysis of HS. The embedded tissues were cut using a microtome.

Table 1. Clinical and Neuropathological Characteristics of Alzheimer's Disease and Non-Demented Control Donor Patients used in the Disaccharide Composition Analysis of Heparan Sulfate

Patient number	Age (years)	Sex	Stage of amyloid deposits (0, A, B, C)*	NFT stage (I–VI)	Cerebral amyloid angiopathy	Vascular risk factors	PMI (hr)
Alzheimer's disease patients							
0508	94	F	C	V	+	CI	43
0512	83	F	C	VI	+	ATH	2
0604	91	F	C	V	–	CI	8
0805	93	F	C	VI	+	CI	27
0810	80	M	C	V	–	CI	15
0811	81	M	C	VI	–	–	8
0814	91	M	C	V	+	–	5
0824	87	F	B	VI	–	–	9
Age-matched non-demented controls							
0707	95	F	A	II	–	MI	4
0710	83	F	A	II	–	CH/CI	24
0601	90	F	B	II	–	MI	4
0802	93	F	A	III	–	CH/CI	20
0704	84	M	B	II	–	CI	3
0807	82	M	0	I	–	CH	8
0908	91	M	A	II	–	–	NA
0903	87	F	0	II	–	CI	7

*0 = none, A = rare or a few, B = mild or moderate, C = numerous or marked.
ATH, atherosclerosis; CH, cerebral hemorrhage; CI, cerebral infarction; F, female; M, male; MI, myocardial infarction; NA, not applicable; NFT, neurofibrillary tangle; PMI, postmortem interval.

Fractionation of Brain Samples

A snap-frozen mouse cortex (~25 mg) was placed in a tube containing 600 μL (30 volume of the tissue weight) of ice-cold Tris-buffered saline (TBS) (20 mmol/L Tris and 137 mmol/L NaCl, pH 7.6) and protease inhibitors (complete protease inhibitor cocktail; Roche Diagnostics, Mannheim, Germany). The tube was placed in a water bath of the Bioruptor ultrasonic vibration (CosmoBio, Tokyo). The tissue was fragmented by sonicating the tube for 15 seconds with the maximum ultrasonic wave output power 4 to 5 times until solid materials in the tube became invisible. The material was ultracentrifuged at 100,000 × *g* for 20 minutes at 4°C. The supernatant was collected and stored frozen as TBS or "TBS soluble fraction." The resulting precipitate was suspended in 600 μL (the same volume as previously described) of TBS containing 1% SDS. The suspension was centrifuged at 12,000 rpm for 20 minutes at room temperature. The resulting supernatant was collected and stored frozen as TBS or "TBS-insoluble/1% SDS-soluble fraction." The protein concentrations of both fractions were measured with a BCA Protein Assay Reagent Kit (Thermo Scientific). Brain cortices were dissected out from 3 Non-Tg or 3 Tg2576 18-month-old mice and then snap frozen. Brain samples were put together, placed on a glass Petri dish, and minced with a blade. The tissues were transferred into a tube containing 1 mL of ice-cold TBS. The tissues were homogenized with a Dounce homogenizer. The homogenate was filtered with a 100-μm nylon mesh. The filtered materials on the mesh were collected and then subjected to the structural analysis described as follows ("vessel-enriched fractions"). Materials filtered through the 100-μm nylon mesh were collected and then analyzed ("non-vasculature fractions"). Methylene blue staining and bright field microscopy confirmed cerebral blood vessels on the filters.

Immunohistochemistry

Fresh mouse brains were embedded in O.C.T. compound (Sakura Finetek, Torrance, CA) and frozen in liquid nitrogen. The brains were stored at −80°C until analysis. Cryostat-cut sections (10-μm thick) were prepared on MAS-coated glass slides (Matsunami, Osaka, Japan), fixed in ice-cold acetone for 15 minutes, and then air-dried for 30 minutes. Sections were incubated with blocking solution (3% bovine serum albumin in PBS) for 15 minutes at RT. Sections were washed twice with PBS and then incubated with a mixture of RB4CD12 (1:100 dilution), rabbit anti-laminin antibody (1:100 dilution, Sigma), and biotinylated 82E1 (1:50 dilution) overnight at 4°C. Then, primary antibodies were detected with Cy3-conjugated monoclonal anti-VSV-G (4 μg/mL), Cy2-conjugated polyclonal goat anti-rabbit IgG (3 μg/mL), and aminomethylcoumarin acetate-conjugated streptavidin (6.8 μg/mL, Jackson ImmunoResearch, West Grove, PA). Sections were mounted in FluorSave Reagent (Merck, Darmstadt, Germany). Digital images were captured by fluorescent microscopy (model BX50, Olympus, Tokyo, Japan) at the same setting for each antibody. The fluorescently stained area was quantitatively determined using Image-Pro Plus software (Media Cybernetics, Bethesda, MD). To determine the effects of the Sulfs and heparinases, 3% bovine serum albumin-blocked sections were pre-treated with 100 μL of a reaction mixture containing 5 μmol HEPES, pH 7.5, 1 μmol $MgCl_2$, and enzymes at 37°C overnight. Recombinant human Sulf-1 (0.4 μg) and human Sulf-2 (0.4 μg) were prepared from conditioned medium of transfected HEK293 cells and used as previously described.[8] For pretreatment with heparitinases, a mixture of 1 mU heparinase I, 0.25 mU heparinase II, and 0.1 mU heparinase III were added to the

reaction mixture. Cy2-conjugated streptavidin was used to detect bound 82E1. Human brain sections (4-μm thickness) were obtained from paraffin-embedded tissue blocks. After deparaffinization and rehydration, endogenous peroxidase activity was quenched with 3% H_2O_2 (Sigma). Sections were subjected to heat-induced epitope retrieval followed by IgG blocking using M.O.M. kit (Vector Laboratories Inc., Burlingame, CA). Sections were incubated with RB4CD12 (1:100 dilution) overnight at 4°C. Bound antibody was detected with horseradish peroxidase-conjugated mouse anti-VSV followed by visualization with diaminobenzidine (3,3′-diaminobenzidinetetrahydrochloride) supplied with the EnVision reagent (Dako Japan, Tokyo, Japan).

Immunoelectron Microscopy

Cryostat-cut sections from 17-month-old Tg2576 mouse brains were prepared on MAS-coated glass slides, fixed in 4% paraformaldehyde for 5 minutes, and then washed with PBS for 1 hour. Sections were incubated with 3% bovine serum albumin for 30 minutes at RT. Diluted RB4CD12 antibody (1:40) was then applied overnight. After washing, diluted rabbit anti-VSV secondary antibody (7.2 μg/mL) was applied for 1 hour. After several washes, diluted goat anti-rabbit IgG antibody coupled with 1.4-nm-diameter tertiary gold particles (1:40) was applied for 30 minutes. The samples were then washed and fixed in 2% glutaraldehyde in 0.1 M sodium cacodylate buffer (pH 7.4) for 3 hours, followed by enlargement of the gold particles with an HQ-Silver Enhancement Kit (Nanoprobes). The specimens were examined in a Hitachi H-7600 transmission electron microscope (Hitachi Koki, Tokyo, Japan).

Immunoblots

The proteins (40 μg per lane) were separated by NuPAGE 3% to 8% polyacrylamide gel electrophoresis (Invitrogen, Carlsbad, CA), and blotted onto a polyvinylidene difluoride membrane (Millipore, Billerica, MA). The membrane was blocked with 5% skim milk/PBS 0.1% Tween for 1 hour at room temperature and then incubated overnight with RB4CD12 antibody (1:500) in TBS 0.1% Tween at 4°C. The membrane was washed and incubated with horseradish peroxidase-conjugated mouse anti-VSV (1:2000) for 1 hour at RT. Bound antibodies were visualized with SuperSignal West Dura Chemiluminescent reagent (Thermo Scientific). Signals were visualized and quantified using a LAS-3000 mini luminescent image analyzer (Fujifilm, Tokyo, Japan).

Preparation and Structural Analysis of HS

There were 100 mg of frozen brain tissues or the cortical vessel residue that remained on filters previously described, which was suspended in 2 mL of 0.2N NaOH and incubated overnight at RT. The samples were neutralized with 4 N HCl and then treated with DNase I and RNase A (0.04 mg/mL each) (Roche Diagnostics) in 50 mmol/L Tris-HCl, pH8.0, 10 mmol/L $MgCl_2$ for 3 hours at 37°C. Subsequently, the samples were treated with actinase E (0.08 mg/mL) (Kaken Pharmaceutical Co., Ltd., Tokyo, Japan) overnight at 37°C. The supernatant was collected by centrifugation at 5000 × *g* at 4°C for 10 minutes after heat inactivation of the enzyme and then mixed with the same volume of 50 mmol/L Tris-HCl, pH 7.2. The HS was purified by DEAE-Sepharose column chromatography.[9] The disaccharide compositions of the HS were determined by reversed-phase ion-pair chromatography with postcolumn fluorescent labeling.

Quantitative Real Time-PCR for Expression of Genes Related to HS Synthesis

Total RNA was extracted from frozen mouse cortices using TRIZol Reagent (Invitrogen). Total RNA (4 μg was used for reverse transcription reaction in 100 μL of buffer with random hexamers, using Superscript II Reverse Transcriptase (Invitrogen). PCR was conducted in duplicate with 20-μL reaction volumes of SYBR Premix Ex TaqII (Takara Bio Inc. Shiga, Japan), 0.2 μmol/L of each primer and 2 μL of the cDNA reaction mixture. PCR was performed using the following parameters: 95°C, 10 seconds, 1 cycle; 95°C, 5 seconds; and 60°C, 30 seconds, 40 cycles. Analysis was performed using sequence detection software supplied with Thermal Cycler Dice Real Time System TP800 (Takara Bio Inc.). mRNA levels of each gene were normalized by comparison to β-actin mRNA levels. Conclusions are drawn from duplicate PCR reactions at least two independent reverse transcription reactions. Primer sequences used in this study are as indicated for *Ndst1*, 5′-GCAGATGGCCCTGAACAAGAA-3′ and 5′-GCACGTGCACAGGGTACACA-3′; for N-deacetylase/*N*-sulfotransferase 2 (*Ndst2*), 5′-TCATCCAGAAGTTCCTGGGTATCAC-3′ and 5′-AGACAGCGAGTCTTACCACCTTCAA-3′; for *Ndst3*, 5′-TCTGGTGTCAGCTGCTGGAAG-3′ and 5′-CACGTTGTGGTCGCGGTAGTAG-3′; for *Ndst4*, 5′-TTGTTCCCAAAGCCAAGATCATTAC-3′ and 5′-TCAGGGCAGCTGGATCTTCA-3′; for *Hs6st1*, 5′-CTGACTGGACCGAACTCACCAA-3′ and 5′-TCTCGCAGCAGGGTGATGTAGTAG-3′; for *Hs6st2*, 5′-AAACTTCAACTCAGGCGCCAAC-3′ and 5′-CTCCATTCACTCAAGTACCGTGACA-3′; for *Hs6st3*, 5′-GACTGGACCGAGCTCACCAA-3′ and 5′-CATGCTTCCATTCGCTCAGGTA-3′; for *Hs2st1*, 5′-GCAAGCACCTCGTTCACCAA-3′ and 5′-CATCTCGTTCCAGGTGGTTATGTTC-3′; for *Sulf1*, 5′-CCACATGGAGTTCACCAACGTC-3′ and 5′-TAGCCGTGGTCCGCAGTGTA-3′; for *Sulf2*, 5′-GAGTACCAGACAGCATGCGAACA-3′ and 5′-TTGGGCACCAGGTTGGAGA-3′; and for *Actb*, 5′-CATCCGTAAAGACCTCTATGCCAAC-3′ and 5′-ATGGAGCCACCGATCCACA-3′.

Statistical Analysis

All data are presented as means ± SD unless noted otherwise. The values were analyzed by unpaired Student's *t*-test using Prism software (GraphPad Software, La Jolla, CA). *P* values less than 0.05 were considered to be statistically significant.

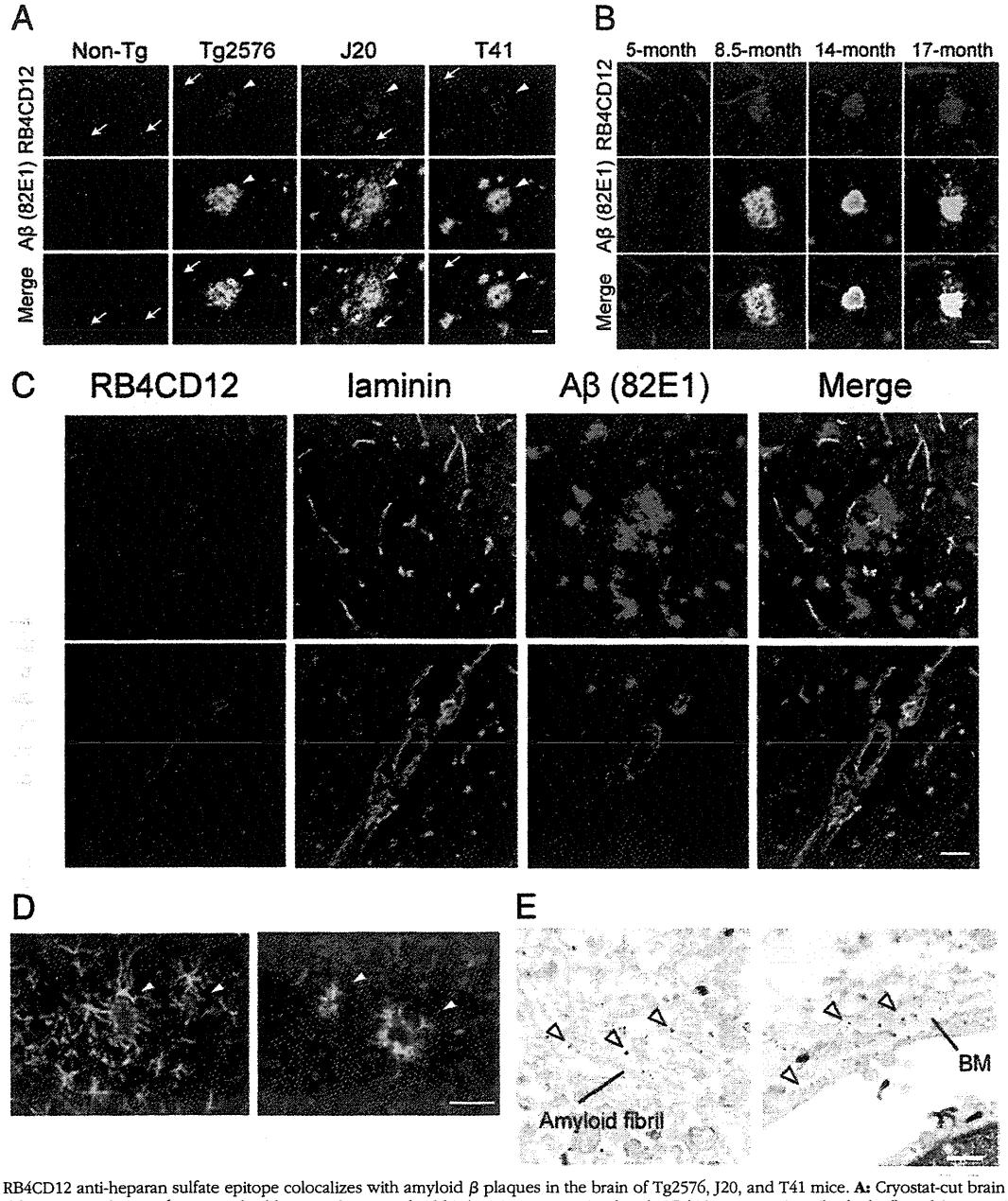

Figure 1. RB4CD12 anti-heparan sulfate epitope colocalizes with amyloid β plaques in the brain of Tg2576, J20, and T41 mice. **A:** Cryostat-cut brain sections of 18-month-old non-Tg and Tg2576, 23-month-old J20, and 12-month-old T41 mice were stained with RB4CD12 anti-HS antibody (red) and 82E1 anti-amyloid β (Aβ) antibody (green). Staining signals in vessels (**arrows**) and amyloid plaques (**arrowheads**) are shown. **B:** Expression of the RB4CD12 epitope and Aβ in aging Tg2576 brain. **C:** Expression of the RB4CD12 epitope, Aβ and laminin, a marker for vessels in the 18-month-old Tg2576 brain. **D:** Co-staining of RB4CD12 anti-HS antibody (red) with cell type-specific antibodies against glial fibrillary acidic protein astrocytes (**left**) or Iba1 microglia (**right**) (green). Co-stained areas are shown in yellow. **E:** Immunoelectron microscopy for the RB4CD12 epitope in amyloid fibrils in the brain of 18-month-old Tg2576 mouse. **Left panel** shows RB4CD12 signals in amyloid fibrils indicated by **arrowheads**. **Right panel** shows RB4CD12 signals in the basement membrane of vessels. BM, basement membrane. Scale bars (in **A**, **C**, and **D**): 50 μm. Scale bars (in **B** and **E**): 20 μm and 500 nm, respectively.

Results

Immunoreactivity of RB4CD12 Anti-Heparan Sulfate is Colocalized with Aβ Plaques in Brains of Transgenic Mouse Models of AD

RB4CD12 scFv antibody recognizes trisulfated disaccharide-containing highly sulfated domains within HS.[8,21] The RB4CD12 epitope has been shown to be present abundantly in the vasculature of the brain in mice.[9] We first analyzed expression of the RB4CD12 epitope in the brain of transgenic mouse models of AD. Tg2576 mice express mutated human amyloid precursor protein in the brain and show numerous Aβ plaques in the cortex and hippocampus.[18] The localization of the RB4CD12 highly sulfated domains in Aβ plaques was observed in an 18-month-old Tg2576 hippocampus (Figure 1A). The RB4CD12 epitope was immunolocalized in both diffuse

and neuritic amyloid plaques in the brain of Tg2576 (Figure 1, A–C). RB4CD12 also detected brain microvessels in Tg2576 mice. No specific staining was observed when RB4CD12 was substituted with MPB49, a non-HS scFv antibody (not shown). We also tested aged J20 and T41, other mouse models of AD. With respect to expression levels of Aβ peptides, Aβ42 is dominant in J20 and T41 mouse brains, whereas Aβ40 is dominant in Tg2576 mouse. We examined brain sections of these model mice immunohistochemically. The RB4CD12 highly sulfated domains were colocalized with Aβ plaques in the hippocampus of 23-month-old J20 and 12-month-old T41 mice (Figure 1A). To analyze age-dependent accumulation of the RB4CD12 epitope in Aβ plaques, we collected Tg2576 brains from 5-, 8.5-, 14- and 17-month-old mice. Aβ plaques were observed in 8.5-, 14- and 17-month-old Tg2576 brains. Cerebral Aβ deposition increases with age. RB4CD12 stained Aβ plaques at these ages (Figure 1B). Next, we investigated vasculature and non-vasculature RB4CD12 epitopes in aged Tg2576 brain by co-staining with antibodies against Aβ and laminin, a marker of vascular basement membranes. Immunoreactivity of RB4CD12 in vascular structure was colocalized with anti-laminin staining signals (Figure 1C). RB4CD12 staining signals that were not associated with signals of anti-laminin antibody predominantly colocalized with anti-Aβ staining signals in the cortex of Tg2576 mice (Figure 1C, upper panels). The RB4CD12 epitope was also observed in the vessel walls of Aβ-positive leptomeningeal vessels (Figure 1C, lower panels). Staining patterns of RB4CD12 were different from the immunoreactivity of glial fibrillary acidic protein, an astrocyte marker, and Iba-1, a microglia marker (Figure 1D). Immunoelectron microscopy confirmed the localization of RB4CD12 epitope within amyloid fibrils and the basement membrane (Figure 1E). The RB4CD12 immunoreactive area that is not colocalized with anti-laminin staining signals was determined by fluorescence microscopy and quantified with computer-aided image analysis. In Tg2576 cortex and hippocampus, RB4CD12-positive but laminin-negative area was increased to fourfold to fivefold of that in non-Tg (Figure 2). In contrast, no change was observed in the cerebellum where no Aβ plaques were observed (Figure 2). We noted that laminin-positive vessels had attenuated diameters and a more ragged profile in Tg2576 cortex and hippocampus (Figure 2).

The RB4CD12 Epitope Is Immunolocalized in Amyloid Plaques in Postmortem Brains of Alzheimer's Disease Patients

We tested RB4CD12 antibody for staining of brains from NDC individuals and AD patients (Table 1). In NDCs, vessel-staining signals were predominantly observed (Figure 3A). In AD entorhinal cortex, amyloid deposits, as well as vessels, were positive for RB4CD12 (Figure 3B). Amyloid deposits and microvessels were also stained with RB4CD12 in AD hippocampus (Figure 3C). Interestingly, some pyramidal neurons in AD hippocampus showed intracellular granular staining (Figure 3D). These intracellular staining signals were detected in a certain number of cells that were positive for hyperphosphorylated microtubule-associated protein tau as revealed by the AT180 monoclonal antibody (see Supplemental Figure S1 at *http://ajp.amjpathol.org*).

Expression of the RB4CD12 Epitope Borne in Molecules with 70–180 kDa Molecular Weights Is Upregulated in the Cortex of Tg2576 Mice

As an extension of the staining results in the mouse and human brain tissues, we wished to determine which proteins contain the RB4CD12 epitope and were differentially expressed in Tg2576 brains. We performed Western blotting for cortex samples, which were fractionated as TBS-insoluble/1% SDS-soluble. Four non-Tg and five Tg2576 mice (20 months old) were examined. Multiple bands were positive for RB4CD12 antibody in both non-Tg and Tg2576 (Figure 4A). We measured intensities of 460 kDa, 180 kDa, 120 kDa, and 100–70 kDa bands by densitometry. There was a 1.3-fold increase in the intensity of overall RB4CD12 recognition determinants in Tg2576 brain extracts compared with non-Tg controls (Figure 4B). Expression levels of RB4CD12 epitopes in bands of 180 kDa, 120 kDa, and 100–70 kDa were increased 1.1- to 1.5-fold in the cortex of Tg2576 mice (Figure 4B). There was no significant change in the intensity of bands of 460 kDa. Syndecan-3 and glypican-1 are HSPGs expressed in glial cells surrounding Aβ plaques of Tg2576 mice.[22] To ascertain whether these proteins are HSPGs that contain the RB4CD12 epitope, we then analyzed their expression. Western blotting revealed the protein bands at 250 to 180 kDa for syndecan-3 and 60 kDa for glypican-1 in the cortex of Tg2576 mice (see Supplemental Figure S2A at *http://ajp.amjpathol.org*). Expression levels of these proteins in the Tg2576 cortex were comparable to those in non-Tg controls (see Supplemental Figure S2B at *http://ajp.amjpathol.org*).

Disaccharide Compositions of HS and Expression Profiles of HS Enzymes in the Cortex of Tg2576 and Postmortem AD

We performed structural analysis of HS chains extracted from mouse and human postmortem brains (Table 1). HS was isolated from the cortex of mice or postmortem human entorhinal cortex. HS was depolymerized into its constituent disaccharides by a mix of bacterial heparitinases. The disaccharide compositions of the HS were determined by reversed-phase ion-pair chromatography. We found that the total HS contents and HS disaccharide compositions in vessel-enriched fractions ("vessel-enriched fr") and non-vessel associated fractions ("non-vasculature fr") were comparable between non-Tg and Tg2576 mice (Figure 4C). In human, the reduction in the proportion of non-sulfated disaccharides reached statistical significance. Total HS contents and percentages of other sulfated disaccharides were comparable between NDC and AD (Figure 4D). To understand possible mechanisms of upregulation of the RB4CD12 epitope in AD mouse brains, we measured mRNA levels of 10 HS modification enzymes by quantitative real time-PCR. HS enzymes include sulfotransferases and extracellular sulfatases. These enzymes are regarded as

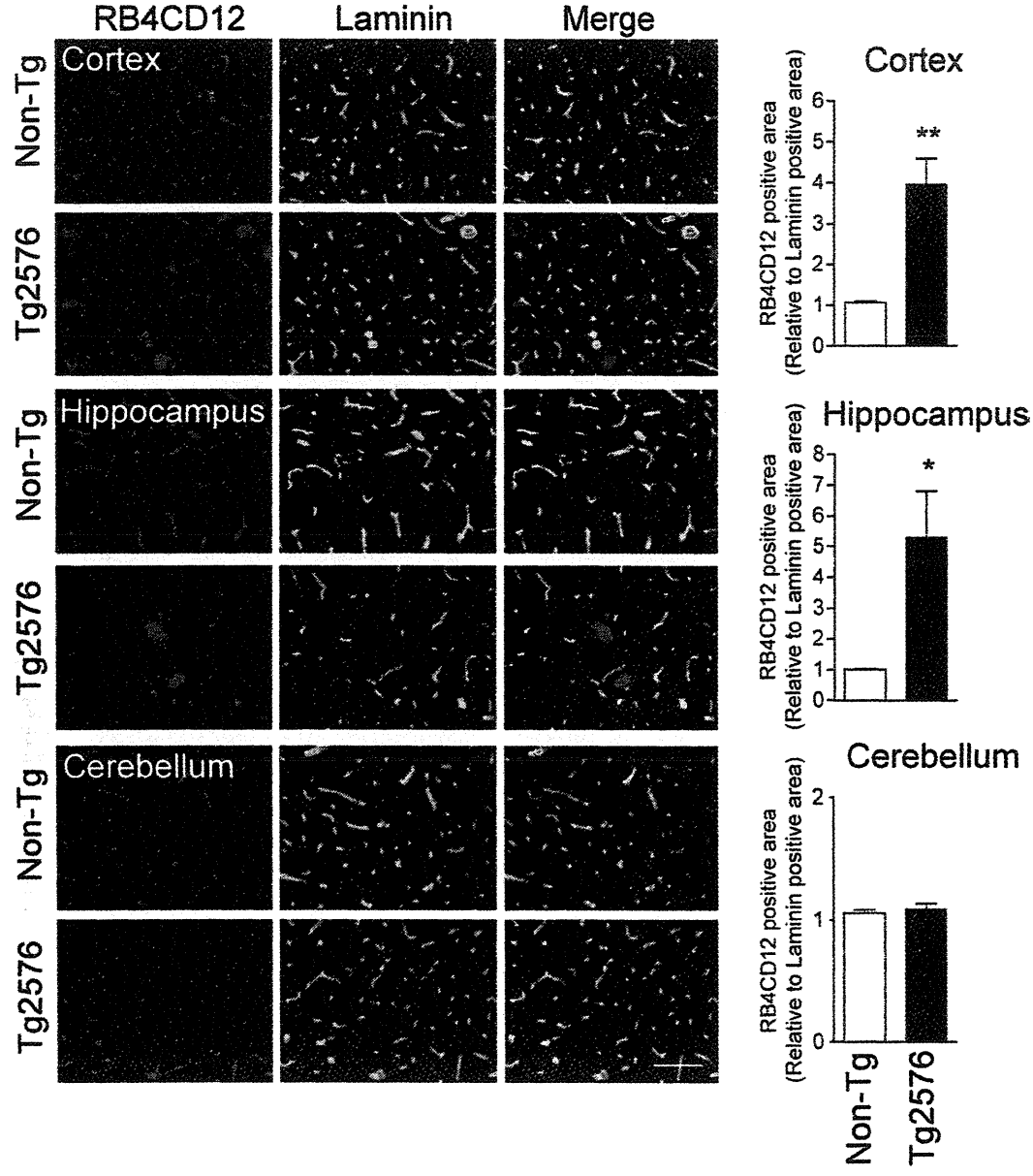

Figure 2. Quantification of the RB4CD12 epitope in nonvascular parenchyma in the brain of Tg2576 mice. Cryostat-cut brain sections of Tg2576 mice were stained with RB4CD12 (red) and anti-laminin (green) antibodies. Laminin is a marker for brain vessels. Nonvascular amyloid β plaques were stained with RB4CD12 antibody in the cortex and hippocampus. Graphs are of semiquantitative analysis of immunohistochemical pictures of RB4CD12 and laminin. RB4CD12-positive areas that were not colocalized with anti-laminin staining signals were calculated. $^{*}P < 0.05$, $^{**}P < 0.01$.

key molecules in the regulation of sulfation of HS. The mRNA level of N-deacetylase/N-sulfotransferase 2 were significantly increased in Tg2576 (24%) (Figure 4E). The mRNA levels of Sulf-1 and Sulf-2 were comparable between non-Tg and Tg2576 mice (Figure 4E).

Sulf-1 and Sulf-2, Extracellular HS Sulfatases, Degrade the RB4CD12 Epitope Accumulated in Amyloid Plaques

Previously, we showed that the treatment of wild-type mouse brain sections with Sulf-1 or Sulf-2 greatly diminished the RB4CD12 epitope abundant in vasculature.[8] To determine whether the RB4CD12 epitope in amyloid plaques is susceptible to Sulf-1 and Sulf-2 and degraded by these enzymes, we treated cryo-cut brain sections of 18-month-old Tg2576 mice with recombinant Sulf-1, Sulf-2, or conditioned medium of MCF-7 breast cancer cells, which secrete native Sulf-2.[23] These treatments substantially reduced the RB4CD12 epitope in sections of Tg2576 brain *ex vivo* (Figure 5). A mixture of bacterial heparinases confirmed that the assay is suitable for *ex vivo* degradation of HS in brain sections and that the observed signals arose from HS (Figure 5). Anti-Aβ staining signals that were colocalized with the RB4CD12 epitope were retained after Sulf treatment (Figure 5).

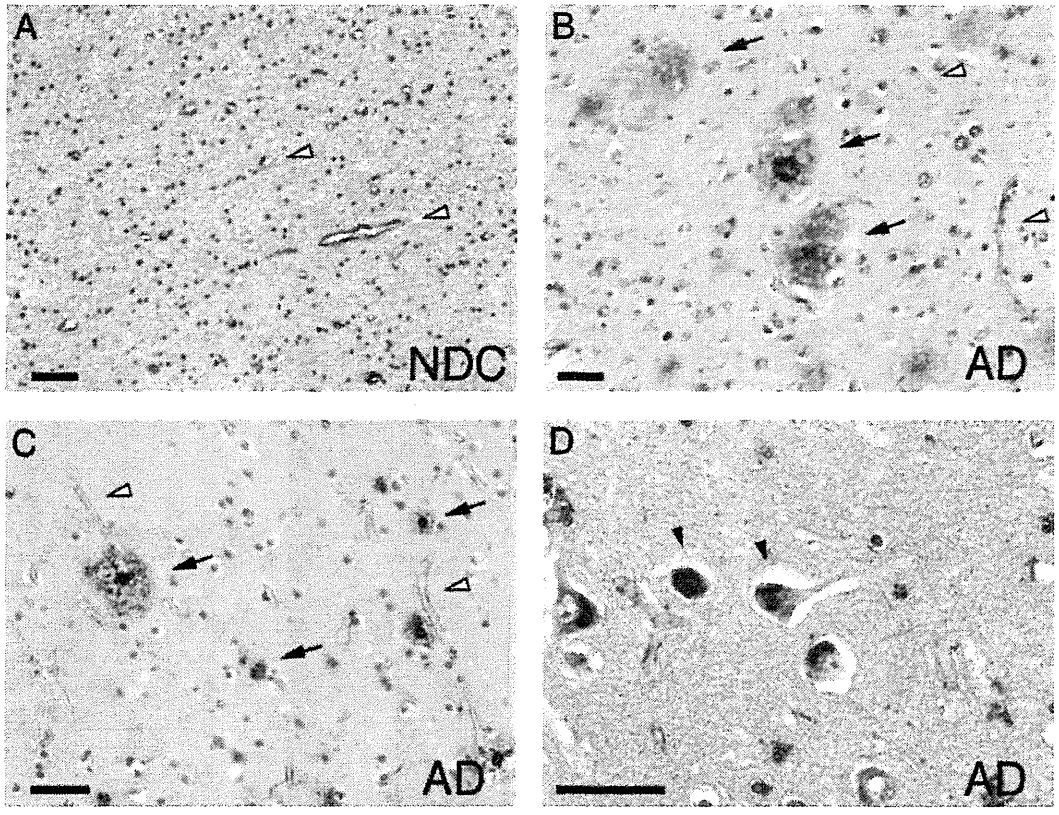

Figure 3. RB4CD12 epitope immunolocalizes in amyloid plaques in the brains of Alzheimer's disease patients. Immunoperoxidase staining for RB4CD12 (brown) in the entorhinal cortex (**A**, **B**) and hippocampus (**C**, **D**). **Open arrowheads** in **A–C** show vessel-staining signals in brains of non-demented control (NDC) and Alzheimer's disease (AD). In AD, amyloid deposits were also positive for RB4CD12 (**arrows** in **B** and **C**). Intracellular RB4CD12-staining signals are seen in some hippocampal neurons of AD (**arrowheads** in **D**). Scale bars: 50 μm.

Discussion

In the present study, we showed that the RB4CD12 epitope is colocalized with amyloid plaques in brains of AD mouse models and patients with AD. Consistent with our previous report,[9] the RB4CD12 epitope was also colocalized with laminin-positive vasculature in brains of mouse models of AD. Quantification analysis revealed that the non-vascular RB4CD12-positive area was increased in the cortex and hippocampus of Tg2576, J20, and T41 AD models. In the cerebellum, where no amyloid plaques were observed in these model mice, RB4CD12 staining was comparable to that in the non-Tg. Morphological alterations of the vasculature observed in the cortex and hippocampus of Tg2576 were consistent with the previous report that Aβ aggregates induce the structural and functional disruption of smooth muscle cells in the vasculature.[24] Results in aging brains of Tg2576 mice suggested that Aβ and the HS highly sulfated domains start accumulation at the same age. Aβ and other self-aggregating peptides share cationic motifs that may be involved in binding to the negative charges of sulfated glycosaminoglycan.[25,26] HS and other glycosaminoglycan chains can stabilize mature fibrils against proteolytic degradation.[27] HS facilitates the formation of fibrils of amylin,[17] apo-serum amyloid A,[28] α-synuclein,[29] prion protein,[30] muscle acylphosphatase,[31] transthyretin,[32] Tau,[33] and Aβ.[34–36] *In vivo* fragmentation of heparan sulfate by heparanase overexpression could protect mice from amyloid protein A amyloidosis.[37] Importantly, the degree of sulfation is critical for enhancement of fibrillogenesis of Aβ.[35] Pathological effects of heparin in Aβ aggregation assays are dependent on sulfate moieties at N- and O-positions.[38] Our findings of selective accumulation of the RB4CD12 epitope in amyloid plaques suggest that highly sulfated domains of HS could play an important role in the progression of Aβ deposition. HSPG facilitates cerebral amyloid deposition, which can be induced exogenously in a rat model.[15] Highly sulfated HS chains could be one candidate for heat-resistant materials present in the brain extract that are essential for exogenous induction of cerebral β-amyloidogenesis in mouse models.[39] Recently, Timmer et al[40] demonstrated that only a minimal number of Aβ plaques (~30%) were co-stained with the epitope of JM403, an anti-HS antibody, in aging brains of APPswe/PS1dE9 model mice. JM403 detects HS subdomains containing the positively charged disaccharide [-glucuronic/iduronic acid-N-unsubstituted glucosamine].[41] Future studies may reveal differential contribution of HS subdomains composed of specific disaccharide structures to AD pathogenesis. Possible involvement of the RB4CD12 epitope existing in laminin-positive vasculature in AD pathogenesis should also be clarified in the future. Interestingly, intraneuronal RB4CD12 staining was observed in the

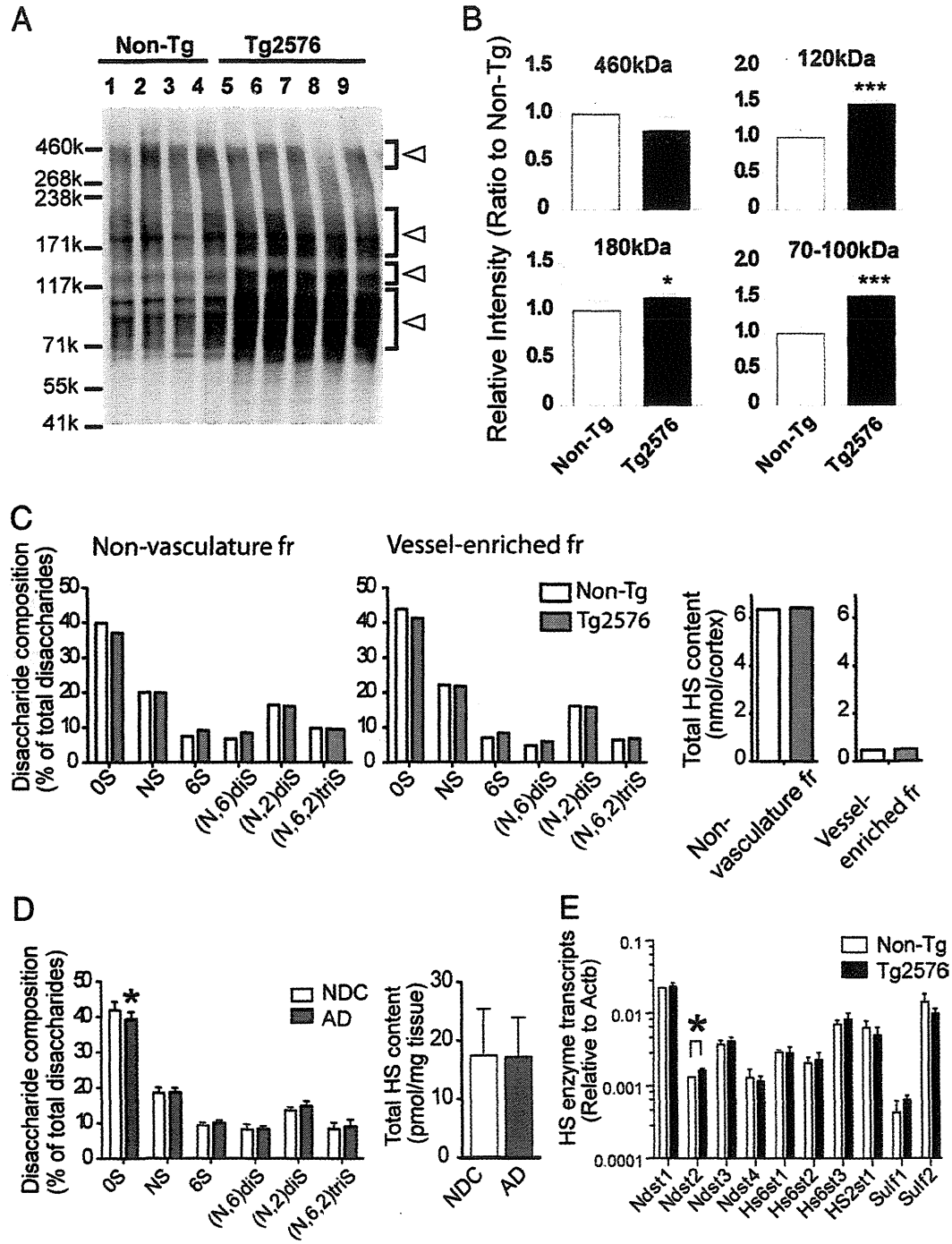

Figure 4. Immunoblotting analysis of the RB4CD12 epitope, disaccharide composition analysis of Heparan sulfate (HS) and quantitative real-time PCR analysis of HS enzymes in the brain of Tg2576 mice. **A:** Tris-buffered saline (TBS)-insoluble/1% SDS-soluble fractions were prepared from tissue homogenates of four 20-month-old Tg2576 (lanes 1–4) and five 20-month-old non-Tg (lanes 5–9) cortices. Immunoblot with RB4CD12 was performed as described in *Materials and Methods.* **B:** Relative intensities of bands with molecular weights of 460 kDa, 180 kDa, 120 kDa, and 70 to 100 kDa indicated by **open arrowheads** in (**A**) were measured. **C:** High performance liquid chromatography analysis determined non-sulfated (0S), monosulfated (NS, 6S), disulfated ([N,6]diS, [N,2]diS) and trisulfated ([N,6,2]triS) disaccharide compositions in non-vasculature fractions and vessel-enriched fractions of 18-month-old non-Tg and Tg2576 cortices. The level of total HS was determined by summing amounts of all disaccharides detected in each fraction. The values are representative of two independent experiments. **D:** HS disaccharide compositions and the level of total HS in the entorhinal cortex of non-demented control (NDC) (n = 8) and Alzheimer's disease (AD) (n = 8) postmortem brains were determined. **E:** Total-RNA from the cerebral cortices of 18-month-old Non-Tg (n = 3) and Tg2576 mice (n = 3) were prepared and tested. mRNA levels of 10 HS modification enzymes were determined by quantitative real-time PCR. $^{*}P < 0.05$, $^{***}P < 0.001$.

hippocampus of AD patients. Microtubule-associated protein Tau is the major protein subunit of intraneuronal neurofibrillary tangles, another neuropathological hallmark of AD.[42] It has been shown that Tau and HS coexist in nerve cells with overt neurofibrillary lesion.[33] The filamentous structures induced by heparin are structurally similar to those found in Alzheimer's disease.[43–45] We have shown that some of RB4CD12

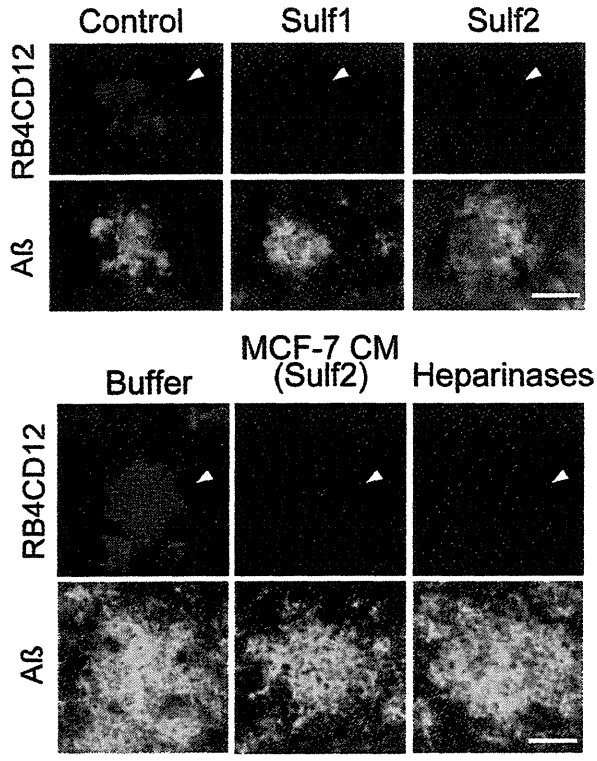

Figure 5. The RB4CD12 epitope in amyloid plaques of Tg2576 mouse brains is degraded *ex vivo* by Sulf-1, Sulf-2 and conditioned medium of Sulf-2-expressing cells. Cryostat-cut consecutive sections of 18-month-old Tg2576 mouse brains were incubated overnight with recombinant human Sulf-1 and Sulf-2 prepared from CM of transfected HEK293 cells (Sulf1, Sulf2), buffer only (Buffer), or CM of MCF-7 human breast cancer cells (MCF-7 CM).[8,23] The Ni-NTA resin-bound materials that were prepared from HEK293 cells transfected with the empty vector were eluted and used (control). A mix of bacterial heparinases (heparinases) served as a positive control. RB4CD12 binding was visualized using a Cy3-conjugated anti-VSV tag antibody (red). Treated sections were co-stained with 82E1 anti-Aβ antibody (green). The data are representative of two independent experiments. **Arrowheads** indicate amyloid plaques. Scale bars: 20 μm.

staining signals were found in cells that were stained with AT180, an antibody against hyperphosphorylated tau. Our results suggest that highly sulfated domains of HS might play a role in the formation of neurofibrillary tangles.

In immunoblots of brain lysates with the RB4CD12 antibody, we detected several RB4CD12-positive bands in non-Tg and Tg2576 mouse brains and found that 180 kDa, 120 kDa, and 100–70 kDa bands were upregulated in the cortex of Tg2576 mice. There were no significant changes in the intensities of 460 kDa bands. Our previous results showed that the RB4CD12 epitope is abundant in the basement membrane of the brain vessels and that the RB4CD12-positive bands were predominantly 460 kDa bands in brain vessel fractions.[9] In our immunohistochemical studies, non-vascular RB4CD12 staining was increased in Tg2576 mice. These results suggest that upregulation of 180 kDa, 120 kDa, and 100–70 kDa bands could contribute to the RB4CD12 staining colocalized with amyloid plaques in Tg2576 mouse brain. Several HSPGs are known to be localized in amyloid plaques.[14,46–49] Because of the high molecular weight (>210 kDa) of agrin and perlecan, it is conceivable that the observed signals in immunoblots might have arisen from other molecules. Syndecan-3 and glypican-1 in glial cells were identified as molecules associated with Aβ deposits.[22] Our Western blotting results suggested that syndecan-3 with the molecular weights of 180 to 250 kDa could be an HSPG that possesses the RB4CD12 epitope. However, we cannot rule out the possibility that degradation products of agrin or perlecan could harbor the RB4CD12 epitope observed in amyloid plaques. We should also pay attention to possible accumulation of HS degradation products catalyzed by nitric oxide.[50]

Unexpectedly, the trisulfated disaccharide composition was not increased in either Tg2576 or human postmortem AD brains. The mechanisms underlying the accumulation of the RB4CD12 highly sulfated domains within HS polysaccharides in non-vasculature amyloid plaques are not clear. There are two possibilities to explain the mechanisms. First, the N-sulfation of glucosamine residues is the initial HS sulfation and the N-sulfated domains are primary sites for further modification.[51] Consecutive occurrence of N-sulfation could be attributable to the formation of trisulfated disaccharide clusters, namely, highly sulfated domains, within HS chains in non-vasculature spaces. Second, translocation of HS that contains the RB4CD12 highly sulfated domains between brain vasculature and non-vasculature could be an explanation for the accumulation of the RB4CD12 epitope in Tg2576 brain parenchyma. Our findings that comparable levels of disaccharide compositions and HS contents in vessel-enriched fractions and non-vasculature fractions in the cortex of Tg2576 were shown and that the mRNA level of N-deacetylase/N-sulfotransferase 2 was increased in the cortex of Tg2576 mouse could support the former possibility. A previous study by Lindahl et al[52] showed altered distribution of N-sulfated glucosamine residues within HS extracted from postmortem AD brain. Highly N-sulfated HS may be involved in the initiation of the aggregation process of Aβ in AD brains.[53] These studies also support the former possibility as an explanation of the mechanisms of accumulation of RB4CD12-positive highly sulfated domains in Aβ plaques. We cannot rule out the possibility that the RB4CD12 epitope is a minor component and that the structural analysis we have performed might not fully detect the minor change. Quantitative analysis for the RB4CD12-positive HS in the cortex would make advances in the study of the mechanisms.

Herein, we found that the RB4CD12 epitope accumulated in amyloid plaques can be degraded by Sulf-1 and Sulf-2 *ex vivo*. It was suggested that the RB4CD12 highly sulfated domains are localized at the surface of amyloid plaques, as these HS degrading enzymes could access and efficiently degrade the epitope. Although the RB4CD12 epitope in amyloid plaques was degraded by the Sulfs, substantial amounts of Aβ were retained in these plaques. This result suggests that the highly sulfated domains of HS universally associated with amyloid deposits in the brain. Accumulation of the RB4CD12 epitope in amyloid plaques could induce excessive entrapment of growth factors at amyloid plaques, which might lead to an imbalance in homeostasis of the brain microenvironment. Increasing evidence points to vascular damage as an early contributor in Alzheimer pathology.[54,55] A recent study suggested that angiogenesis

might be impaired in AD model mice,[56] despite the fact that the levels of pro-angiogenic growth factors (eg, vascular endothelial growth factor [VEGF]) are elevated in AD brains.[57–59] VEGF binds to immobilized heparin and can be stored in the extracellular space by binding to HS and HSPG.[23,60] Heparin-bound VEGF is mobilized by the action of Sulf-2, which exerts pro-angiogenic activity.[23,61] VEGF is found to be associated with amyloid plaques in AD, but not non-AD brain.[62] Our results also suggested that the highly sulfated domains could be involved in sequestration of VEGF within amyloid plaques and vascular damage in AD through perturbation in the supply of pro-angiogenic growth factors. Aberrant angiogenesis could induce neurovascular uncoupling, which ultimately leads to synaptic dysfunction.[63] In summary, we provide evidence that highly sulfated domains recognized by RB4CD12 accumulated in amyloid plaques of brains of AD model mice and patients with AD. Further studies to investigate the roles of the highly sulfated HS domains with special regard to angiogenesis in AD pathology will be needed.

Acknowledgments

We thank Steven Rosen and Yoshiko Takeda-Uchimura for their helpful suggestions and discussions. We also thank Kuniko Takanose, Noriko Sugaya, and Hudson Johns for their technical assistance. We are grateful to Yoshio Hashizume and Takayuki Yamamoto for their diagnostic examination and support.

References

1. Bernfield M, Gotte M, Park PW, Reizes O, Fitzgerald ML, Lincecum J, Zako M: Functions of cell surface heparan sulfate proteoglycans. Annu Rev Biochem 1999, 68:729–777
2. Esko JD, Lindahl U: Molecular diversity of heparan sulfate. J Clin Invest 2001, 108:169–173
3. Gallagher JT: Heparan sulfate: growth control with a restricted sequence menu. J Clin Invest 2001, 108:357–361
4. Nakato H, Kimata K: Heparan sulfate fine structure and specificity of proteoglycan functions. Biochim Biophys Acta 2002, 1573:312–318
5. Parish CR: The role of heparan sulphate in inflammation. Nat Rev Immunol 2006, 6:633–643
6. Bishop JR, Schuksz M, Esko JD: Heparan sulphate proteoglycans fine-tune mammalian physiology. Nature 2007, 446:1030–1037
7. Dennissen MA, Jenniskens GJ, Pieffers M, Versteeg EM, Petitou M, Veerkamp JH, van Kuppevelt TH: Large, tissue-regulated domain diversity of heparan sulfates demonstrated by phage display antibodies. J Biol Chem 2002, 277:10982–10986
8. Hossain MM, Hosono-Fukao T, Tang R, Sugaya N, van Kuppevelt TH, Jenniskens GJ, Kimata K, Rosen SD, Uchimura K: Direct detection of HSulf-1 and HSulf-2 activities on extracellular heparan sulfate and their inhibition by PI-88. Glycobiology 2010, 20:175–186
9. Hosono-Fukao T, Ohtake-Niimi S, Nishitsuji K, Hossain MM, van Kuppevelt TH, Michikawa M, Uchimura K: RB4CD12 epitope expression and heparan sulfate disaccharide composition in brain vasculature. J Neurosci Res 2011, 89:1840–1848
10. Esko JD, Selleck SB: Order out of chaos: assembly of ligand binding sites in heparan sulfate. Annu Rev Biochem 2002, 71:435–471
11. Saad OM, Ebel H, Uchimura K, Rosen SD, Bertozzi CR, Leary JA: Compositional profiling of heparin/heparan sulfate using mass spectrometry: assay for specificity of a novel extracellular human endosulfatase. Glycobiology 2005, 15:818–826
12. Morimoto-Tomita M, Uchimura K, Werb Z, Hemmerich S, Rosen SD: Cloning and characterization of two extracellular heparin-degrading endosulfatases in mice and humans. J Biol Chem 2002, 277:49175–49185
13. Snow AD, Mar H, Nochlin D, Kimata K, Kato M, Suzuki S, Hassell J, Wight TN: The presence of heparan sulfate proteoglycans in the neuritic plaques and congophilic angiopathy in Alzheimer's disease. Am J Pathol 1988, 133:456–463
14. Snow AD, Sekiguchi RT, Nochlin D, Kalaria RN, Kimata K: Heparan sulfate proteoglycan in diffuse plaques of hippocampus but not of cerebellum in Alzheimer's disease brain. Am J Pathol 1994, 144: 337–347
15. Snow AD, Sekiguchi R, Nochlin D, Fraser P, Kimata K, Mizutani A, Arai M, Schreier WA, Morgan DG: An important role of heparan sulfate proteoglycan (Perlecan) in a model system for the deposition and persistence of fibrillar A beta-amyloid in rat brain. Neuron 1994, 12:219–234
16. van Horssen J, Wesseling P, van den Heuvel LP, de Waal RM, Verbeek MM: Heparan sulphate proteoglycans in Alzheimer's disease and amyloid-related disorders. Lancet Neurol 2003, 2:482–492
17. Watson DJ, Lander AD, Selkoe DJ: Heparin-binding properties of the amyloidogenic peptides Abeta and amylin. Dependence on aggregation state and inhibition by Congo red. J Biol Chem 1997, 272: 31617–31624
18. Hsiao K, Chapman P, Nilsen S, Eckman C, Harigaya Y, Younkin S, Yang F, Cole G: Correlative memory deficits. A beta elevation, and amyloid plaques in transgenic mice, Science 1996, 274:99–102
19. Mucke L, Masliah E, Yu GQ, Mallory M, Rockenstein EM, Tatsuno G, Hu K, Kholodenko D, Johnson-Wood K, McConlogue L: High-level neuronal expression of abeta 1–42 in wild-type human amyloid protein precursor transgenic mice: synaptotoxicity without plaque formation. J Neurosci 2000, 20:4050–4058
20. Rockenstein E, Mallory M, Mante M, Sisk A, Masliaha E: Early formation of mature amyloid-beta protein deposits in a mutant APP transgenic model depends on levels of A beta(1–42). J Neurosci Res 2001, 66:573–582
21. Jenniskens GJ, Oosterhof A, Brandwijk R, Veerkamp JH, van Kuppevelt TH: Heparan sulfate heterogeneity in skeletal muscle basal lamina: demonstration by phage display-derived antibodies. J Neurosci 2000, 20:4099–4111
22. O'Callaghan P, Sandwall E, Li JP, Yu H, Ravid R, Guan ZZ, van Kuppevelt TH, Nilsson LN, Ingelsson M, Hyman BT, Kalimo H, Lindahl U, Lannfelt L, Zhang X: Heparan sulfate accumulation with Abeta deposits in Alzheimer's disease and Tg2576 mice is contributed by glial cells. Brain Pathol 2008, 18:548–561
23. Uchimura K, Morimoto-Tomita M, Bistrup A, Li J, Lyon M, Gallagher J, Werb Z, Rosen SD: HSulf-2, an extracellular endoglucosamine-6-sulfatase, selectively mobilizes heparin-bound growth factors and chemokines: effects on VEGF. FGF-1, and SDF-1, BMC Biochem 2006, 7:2
24. Christie R, Yamada M, Moskowitz M, Hyman B: Structural and functional disruption of vascular smooth muscle cells in a transgenic mouse model of amyloid angiopathy. Am J Pathol 2001, 158:1065–1071
25. Diaz-Nido J, Wandosell F, Avila J: Glycosaminoglycans and beta-amyloid, prion and tau peptides in neurodegenerative diseases. Peptides 2002, 23:1323–1332
26. McLaurin J, Fraser PE: Effect of amino-acid substitutions on Alzheimer's amyloid-beta peptide-glycosaminoglycan interactions. Eur J Biochem 2000, 267:6353–6361
27. Gupta-Bansal R, Frederickson RC, Brunden KR: Proteoglycan-mediated inhibition of A beta proteolysis. A potential cause of senile plaque accumulation, J Biol Chem 1995, 270:18666–18671
28. Ancsin JB, Kisilevsky R: The heparin/heparan sulfate-binding site on apo-serum amyloid A. Implications for the therapeutic intervention of amyloidosis, J Biol Chem 1999, 274:7172–7181
29. Cohlberg JA, Li J, Uversky VN, Fink AL: Heparin and other glycosaminoglycans stimulate the formation of amyloid fibrils from alpha-synuclein in vitro. Biochemistry 2002, 41:1502–1511
30. Supattapone S: Prion protein conversion in vitro. J Mol Med 2004, 82:348–356
31. Motamedi-Shad N, Monsellier E, Torrassa S, Relini A, Chiti F: Kinetic analysis of amyloid formation in the presence of heparan sulfate: faster unfolding and change of pathway. J Biol Chem 2009, 284: 29921–29934

32. Noborn F, O'Callaghan P, Hermansson E, Zhang X, Ancsin JB, Damas AM, Dacklin I, Presto J, Johansson J, Saraiva MJ, Lundgren E, Kisilevsky R, Westermark P, Li JP: Heparan sulfate/heparin promotes transthyretin fibrillization through selective binding to a basic motif in the protein. Proc Natl Acad Sci USA 2011, 108:5584–5589
33. Goedert M, Jakes R, Spillantini MG, Hasegawa M, Smith MJ, Crowther RA: Assembly of microtubule-associated protein tau into Alzheimer-like filaments induced by sulphated glycosaminoglycans. Nature 1996, 383:550–553
34. McLaurin J, Franklin T, Zhang X, Deng J, Fraser PE: Interactions of Alzheimer amyloid-beta peptides with glycosaminoglycans effects on fibril nucleation and growth. Eur J Biochem 1999, 266:1101–1110
35. Castillo GM, Lukito W, Wight TN, Snow AD: The sulfate moieties of glycosaminoglycans are critical for the enhancement of beta-amyloid protein fibril formation. J Neurochem 1999, 72:1681–1687
36. Valle-Delgado JJ, Alfonso-Prieto M, de Groot NS, Ventura S, Samitier J, Rovira C, Fernandez-Busquets X: Modulation of Abeta42 fibrillogenesis by glycosaminoglycan structure. FASEB J 2010, 24:4250–4261
37. Li JP, Galvis ML, Gong F, Zhang X, Zcharia E, Metzger S, Vlodavsky I, Kisilevsky R, Lindahl U: In vivo fragmentation of heparan sulfate by heparanase overexpression renders mice resistant to amyloid protein A amyloidosis. Proc Natl Acad Sci USA 2005, 102:6473–6477
38. Timmer NM, Schirris TJ, Bruinsma IB, Otte-Holler I, van Kuppevelt TH, de Waal RM, Verbeek MM: Aggregation and cytotoxic properties towards cultured cerebrovascular cells of Dutch-mutated Abeta40 (DAbeta(1–40)) are modulated by sulfate moieties of heparin. Neurosci Res 2010, 66:380–389
39. Meyer-Luehmann M, Coomaraswamy J, Bolmont T, Kaeser S, Schaefer C, Kilger E, Neuenschwander A, Abramowski D, Frey P, Jaton AL, Vigouret JM, Paganetti P, Walsh DM, Mathews PM, Ghiso J, Staufenbiel M, Walker LC, Jucker M: Exogenous induction of cerebral beta-amyloidogenesis is governed by agent and host. Science 2006, 313:1781–1784
40. Timmer NM, Herbert MK, Kleinovink JW, Kiliaan AJ, De Waal RM, Verbeek MM: Limited expression of heparan sulphate proteoglycans associated with Abeta deposits in the APPswe/PS1dE9 mouse model for Alzheimer's disease. Neuropathol Appl Neurobiol 2010, 36:478–486
41. van den Born J, Salmivirta K, Henttinen T, Ostman N, Ishimaru T, Miyaura S, Yoshida K, Salmivirta M: Novel heparan sulfate structures revealed by monoclonal antibodies. J Biol Chem 2005, 280:20516–20523
42. Skovronsky DM, Lee VM, Trojanowski JQ: Neurodegenerative diseases: new concepts of pathogenesis and their therapeutic implications. Annu Rev Pathol 2006, 1:151–170
43. Kuret J, Chirita CN, Congdon EE, Kannanayakal T, Li G, Necula M, Yin H, Zhong Q: Pathways of tau fibrillization. Biochim Biophys Acta 2005, 1739:167–178
44. Perez M, Valpuesta JM, Medina M, Montejo de Garcini E, Avila J: Polymerization of tau into filaments in the presence of heparin: the minimal sequence required for tau-tau interaction. J Neurochem 1996, 67:1183–1190
45. Zhu HL, Fernandez C, Fan JB, Shewmaker F, Chen J, Minton AP, Liang Y: Quantitative characterization of heparin binding to Tau protein: implication for inducer-mediated Tau filament formation. J Biol Chem 2010, 285:3592–3599
46. Van Gool D, David G, Lammens M, Baro F, Dom R: Heparan sulfate expression patterns in the amyloid deposits of patients with Alzheimer's and Lewy body type dementia. Dementia 1993, 4:308–314
47. Donahue JE, Berzin TM, Rafii MS, Glass DJ, Yancopoulos GD, Fallon JR, Stopa EG: Agrin in Alzheimer's disease: altered solubility and abnormal distribution within microvasculature and brain parenchyma, Proc Natl Acad Sci USA 1999, 96:6468–6472
48. Verbeek MM, Otte-Holler I, van den Born J, van den Heuvel LP, David G, Wesseling P, de Waal RM: Agrin is a major heparan sulfate proteoglycan accumulating in Alzheimer's disease brain. Am J Pathol 1999, 155:2115–2125
49. van Horssen J, Otte-Holler I, David G, Maat-Schieman ML, van den Heuvel LP, Wesseling P, de Waal RM, Verbeek MM: Heparan sulfate proteoglycan expression in cerebrovascular amyloid beta deposits in Alzheimer's disease and hereditary cerebral hemorrhage with amyloidosis (Dutch) brains. Acta Neuropathol 2001, 102:604–614
50. Cappai R, Cheng F, Ciccotosto GD, Needham BE, Masters CL, Multhaup G, Fransson LA, Mani K: The amyloid precursor protein (APP) of Alzheimer disease and its paralog. APLP2, modulate the Cu/Zn-Nitric Oxide-catalyzed degradation of glypican-1 heparan sulfate in vivo, J Biol Chem 2005, 280:13913–13920
51. Carlsson P, Presto J, Spillmann D, Lindahl U, Kjellen L: Heparin/heparan sulfate biosynthesis: processive formation of N-sulfated domains. J Biol Chem 2008, 283:20008–20014
52. Lindahl B, Eriksson L, Lindahl U: Structure of heparan sulphate from human brain, with special regard to Alzheimer's disease, Biochem J 1995, 306 (Pt 1):177–184
53. Bruinsma IB, te Riet L, Gevers T, ten Dam GB, van Kuppevelt TH, David G, Kusters B, de Waal RM, Verbeek MM: Sulfation of heparan sulfate associated with amyloid-beta plaques in patients with Alzheimer's disease. Acta Neuropathol 2010, 119:211–220
54. Bailey TL, Rivara CB, Rocher AB, Hof PR: The nature and effects of cortical microvascular pathology in aging and Alzheimer's disease. Neurol Res 2004, 26:573–578
55. Meyer EP, Ulmann-Schuler A, Staufenbiel M, Krucker T: Altered morphology and 3D architecture of brain vasculature in a mouse model for Alzheimer's disease, Proc Natl Acad Sci USA 2008, 105:3587–3592
56. Paris D, Ganey N, Banasiak M, Laporte V, Patel N, Mullan M, Murphy SF, Yee GT, Bachmeier C, Ganey C, Beaulieu-Abdelahad D, Mathura VS, Brem S: Impaired orthotopic glioma growth and vascularization in transgenic mouse models of Alzheimer's disease. J Neurosci 2010, 30:11251–11258
57. Kalaria RN, Cohen DL, Premkumar DR, Nag S, LaManna JC, Lust WD: Vascular endothelial growth factor in Alzheimer's disease and experimental cerebral ischemia. Brain Res Mol Brain Res 1998, 62:101–105
58. Tarkowski E, Issa R, Sjogren M, Wallin A, Blennow K, Tarkowski A, Kumar P: Increased intrathecal levels of the angiogenic factors VEGF and TGF-beta in Alzheimer's disease and vascular dementia. Neurobiol Aging 2002, 23:237–243
59. Siedlak SL, Cras P, Kawai M, Richey P, Perry G: Basic fibroblast growth factor binding is a marker for extracellular neurofibrillary tangles in Alzheimer disease. J Histochem Cytochem 1991, 39:899–904
60. Iozzo RV: Matrix proteoglycans: from molecular design to cellular function. Annu Rev Biochem 1998, 67:609–652
61. Morimoto-Tomita M, Uchimura K, Bistrup A, Lum DH, Egeblad M, Boudreau N, Werb Z, Rosen SD: Sulf-2, a proangiogenic heparan sulfate endosulfatase, is upregulated in breast cancer. Neoplasia 2005, 7:1001–1010
62. Ryu JK, Cho T, Choi HB, Wang YT, McLarnon JG: Microglial VEGF receptor response is an integral chemotactic component in Alzheimer's disease pathology. J Neurosci 2009, 29:3–13
63. Zlokovic BV: Neurovascular mechanisms of Alzheimer's neurodegeneration. Trends Neurosci 2005, 28:202–208